Keystone engineering enables collective range expansion in microbial communities

Emrah Şimşek[1,2*], César A. Villalobos[1,2,9], Kinshuk Sahu[1,2,9], Zhengqing Zhou[1,2], Nan Luo[1,8], Dongheon Lee[1,2], Helena R. Ma[1,2], Deverick J. Anderson[5,6], Charlotte T. Lee[2,7], and Lingchong You[1,2,3,4*]

[1]Department of Biomedical Engineering, Duke University, Durham, NC, 27708

[2]Center for Quantitative Biodesign, Duke University, Durham, NC, 27708

[3]Center for Genomic and Computational Biology, Duke University, Durham, NC, 27708

[4]Department of Molecular Genetics and Microbiology, Duke University School of Medicine, Durham, NC, 27708

[5]Division of Infectious Diseases, Department of Medicine, Duke University School of Medicine, Durham, NC, USA

[6]Duke Center for Antimicrobial Stewardship and Infection Prevention, Duke University School of Medicine, Durham, NC, USA

[7]Department of Biology, Duke University, Durham, NC, 27708

[8]Present address: Shenzhen Institutes of Advanced Technology, Chinese Academy of Sciences, Shenzhen 518055, China

[9]These two authors contributed equally.

[*]Corresponding authors, E-mail: esimsek32@gmail.com, you@duke.edu

Abstract

Keystone engineers profoundly influence microbial communities by altering their shared environment, often by modifying key resources. Here, we show that in an antibiotic-treated microbial community, bacterial spread is controlled by keystone engineering affecting dispersal—an effect hidden in well-mixed environments. Focusing on two pathogens, non-motile *Klebsiella pneumoniae* and motile *Pseudomonas aeruginosa*, we found that both tolerate a β-lactam antibiotic, with *Pseudomonas* being more resilient and dominating in well-mixed cultures. During range expansion, however, the antibiotic inhibits *Pseudomonas*' ability to spread unless it is near *Klebsiella*— *Klebsiella* degrades the antibiotic to create a "clear zone" that allows *Pseudomonas* to expand, at the expense of *Klebsiella*'s own growth, thus acting as a keystone engineer. As *Pseudomonas* spreads, it competitively suppresses *Klebsiella*. Our modeling and experimental analyses reveal that this keystone effect operates at a millimeter scale. We also observed similar keystone engineering by a *Bacillus* species isolated from a hospital sink, in both pairwise and eight-member bacterial communities with its co-isolates. These findings suggest that spatially explicit experiments are essential to understand certain keystone engineering mechanisms and have implications for surface-associated microbial communities like biofilms, as well as for diagnosing and treating polymicrobial infections involving drug-degrading, non-motile (e.g., *Klebsiella*), and drug-tolerant, motile (e.g., *Pseudomonas*) bacteria.

Introduction

A keystone species has a disproportionately large impact on its community relative to its abundance[1,2]. For example, removing the sea star *Pisaster ochraceous* drastically reduces biodiversity in its ecosystem because it allows mussel, its prey, to overgrow[1]. An ecosystem engineer affects other species in its community by modifying their environment. For example, beavers shape freshwater habitats that benefit many other species[3,4]. A species that meets both definitions is called a *keystone engineer*[5].

In microbial communities, keystone engineers are critical for maintaining biodiversity[6,7] and community functioning[8-13], including their impact on human health[14-17]. The keystone species concept originated in natural communities, but the inherent complexity of the latter makes it challenging to uncover their underlying ecological mechanisms. To alleviate this challenge, simplified microbial communities with two to several members have been assembled to extract fundamental mechanistic insights, which can then be tested in increasingly complex communities[18]. Examples include predicting large community outcomes from pairwise interactions[19], revealing limitations of pairwise information for larger communities[20], demonstrating how interspecies interactions during chemotaxis and growth shape marine community assembly[21], showing bioelectric signals mediates interspecies attractive interactions[22], and illustrating how transient invaders can trigger state switching in a two-member community through pH modification[23]. This approach has also revealed keystone roles for bacteria in shaping community composition[7,24], stability[25], biomass production[12,13], biofilm formation[26], pathogen resistance[25], and antimicrobial tolerance[26,27].

Microbial keystone engineers often play their role by breaking down complex resources into products utilizable by other microbes[14,17,24,28-31]. This role can also entail changing the environmental pH[12,24] or modulating the host immune response[15,16,32,33]. For instance, despite its low abundance, *Porphyromonas gingivalis* acts as a keystone that promotes overgrowth of the oral microbiota, which can cause inflammation[16].

Whether a microbe is a keystone engineer depends on context. For instance, in a synthetic mouse gut microbiota, *Bacteroides caecimuris* serves as a keystone engineer only when the polysaccharide inulin is the carbohydrate source[24], as *B. caecimuris* inhibits the growth of other species by acidifying the culture through inulin fermentation[24]. Likewise, *Bacteroides uniformis*

can benefit or compete with butyrate-producing gut bacteria depending on the available carbohydrate sources[31].

While previous studies on keystone engineering have focused predominantly on growth or community structure[14-17,24,28-33], spatial structure is a ubiquitous environmental context for microbes. Many microbes live in spatially structured communities, such as biofilms[34-36]. In such an environment, survival depends on both mobility and effectiveness in nutrient utilization[37-40]. The mobility can be intrinsic or through interactions with other community members. For example, *Escherichia coli* can be transported by *Paenibacillus vortex*[41], and *Pseudomonas aeruginosa* variants hitchhike on shared biosurfactants[42,43]. Biosurfactant production enables collective spatial expansion (called swarming) but comes at a significant growth cost, and cheater variants that do not produce biosurfactants can destabilize this strategy during a prolonged spatial expansion of a population[43]. When invading a spatial environment, *Pseudomonas'* biosurfactants can enable the displacement of competing *Klebsiella*, which previously colonized the environment[44]. These examples underscore the critical need for spatially explicit experiments to uncover microbial interactions. However, due to the lack of such well-controlled experiments, keystone engineering in the context of spatial expansion has not been demonstrated before.

Here, combining mathematical modeling and experiments, we reveal that in a microbial community treated with a β-lactam antibiotic, an immotile species acts as a keystone engineer enabling the spatial expansion of a motile species when sufficiently close. The immotile species detoxifies the environment by degrading the antibiotic, which would otherwise suppress the dispersal—but not the growth—of the motile species. This enables the motile species to expand, and subsequently suppress the growth of the immotile species through an apparent competition, reducing it to a minority. These dynamics constitute keystone engineering by the immotile species, which has a disproportionately large driving role on the spatial expansion of its community compared to its extremely low final relative abundance.

We demonstrated this keystone engineering in two pairwise communities: 1) clinical isolates of β-lactamase (Bla)-producing *Klebsiella pneumoniae* (*Klebsiella*) as the keystone engineer and *Pseudomonas aeruginosa* (*Pseudomonas*) as the motile species under cefotaxime (CTX) treatment, and 2) a nonpathogenic *Bacillus paranthracis* (Bp) with Bla genes (Supplementary Table 1) as the keystone engineer and another, motile *Pseudomonas* strain (Pa22), co-isolated from the same hospital sink, under carbenicillin (CB) treatment. Finally, we

114 demonstrated the applicability of Bp's keystone engineering on Pa22 in a synthetic community
115 with six additional isolates from the same sink sample.
116
117 Based on our results, we hypothesize that a pathogen could appear responsible for a β-
118 lactam resistant infection even though it does not encode Bla or degrade β-lactams (e.g.,
119 *Pseudomonas*), potentially leading to misleading diagnoses. Furthermore, our findings have
120 broader implications for biofilm growth in mixed communities of pathogenic and nonpathogenic
121 microbes in natural environments, such as hospital sinks.
122
123
124 **Results**
125 ***Klebsiella* enabled *Pseudomonas* range expansion under β-lactam treatment at its own**
126 **expense.**
127 We tested the effect of a β-lactam antibiotic (CTX) treatment on the growth (i.e., biomass
128 production) of *Pseudomonas aeruginosa* PA14 (*Pseudomonas*) and a Bla-producing clinical
129 isolate of *Klebsiella pneumoniae* (*Klebsiella*)[45] in well-mixed liquid cultures. *Pseudomonas* and
130 *Klebsiella* are prevalent pathogens in many common infection types[46,47] (Supplementary Fig. 1),
131 can co-colonize patients[48], and co-occur at human infection sites[49] or urinary catheters[50,51],
132 suggesting that they have a strong niche overlap, making their community experiments clinically
133 and ecologically relevant. We first grew *Klebsiella* and *Pseudomonas* in well-mixed pure cultures
134 without or with CTX (2.5 μg/ml) (Fig. 1a). Both species tolerated the CTX treatment, which
135 reduced the biomass production of *Klebsiella* and *Pseudomonas* by 46% and 26%, respectively,
136 when measured after 27 h (Fig. 1a, bottom). *Klebsiella* grew ~ 1.3-times faster than *Pseudomonas*
137 without antibiotics (during the first 6 h) (Fig. 1a, top). With the CTX treatment, *Klebsiella* growth
138 became detectable only after ~ 11 h of incubation (Fig. 1a, bottom), while *Pseudomonas* growth
139 was virtually unaffected (Fig. 1a).
140
141 The results above show that *Klebsiella* grew faster without antibiotic treatment, whereas
142 *Pseudomonas* grew faster under the CTX treatment. When grown as a well-mixed pure culture,
143 each species produced less biomass in medium conditioned by the other species than in
144 unconditioned medium, demonstrating competition between the two species (Supplementary Fig.
145 2). If the two species primarily interact through competition in well-mixed cocultures, we expect
146 the dominance of *Klebsiella* without the CTX treatment and the dominance of *Pseudomonas* with
147 the CTX treatment. To this end, we tested the growth of mix cultures, each starting with equal
148 fractions of *Klebsiella* and *Pseudomonas*, with or without CTX treatment. Indeed, without CTX

149 treatment, *Klebsiella* reached a relative abundance of 75.0% after 27 h (Fig. 1b, top). With CTX
150 (2.5 μg/ml) treatment, *Pseudomonas* reached a relative abundance of 99.9% after 27 h (Fig. 1b,
151 bottom).
152
153 We then examined the two species and their interactions on an agar surface where
154 *Pseudomonas* could exhibit swarming motility[52]. We tested the effect of the β-lactam antibiotic
155 CTX (2.5 μg/ml) on pure cultures of *Pseudomonas* or *Klebsiella* by inoculating them on agar and
156 measuring their colonized areas and biomasses after 24 h of incubation (Fig. 1c; Supplementary
157 Fig. 3, Supplementary Fig. 4a). The CTX treatment suppressed *Pseudomonas* growth by 28-fold
158 when measured by colony areas (Fig. 1c; Supplementary Fig. 3), or 22-fold when measured by
159 biomass (Supplementary Fig. 4a). This result is consistent with the studies that showed that
160 *Pseudomonas*' swarming is inhibited by antibiotic treatment[53,54]. In contrast, the CTX treatment
161 did not significantly affect *Klebsiella* colony growth (Fig. 1c; Supplementary Fig. 3; Supplementary
162 Fig. 4a). In both cases, *Klebsiella* colonies were smaller than those of *Pseudomonas* colonies
163 (Fig. 1c; Supplementary Fig. 3).
164
165 We next measured the growth of a coculture starting with equal biomasses of the two
166 species under the CTX treatment. The coculture colonized a 7.4-fold larger area and produced
167 6.2-fold greater biomass compared to *Pseudomonas* alone (Fig. 1c,d; Supplementary Fig. 3;
168 Supplementary Fig. 4a). Without antibiotic treatment, *Pseudomonas* alone grew better than a
169 mixture (Fig. 1c,d; Supplementary Fig. 3; Supplementary Fig. 4a), though the difference was
170 statistically insignificant (A two-sample t-test assuming unequal variances (Welch's t-test) was
171 used to test the null hypothesis of no difference. The corresponding two-tailed *P*–values are 0.081
172 and 0.25 for colonized area and biomass, respectively). The collective range expansion by
173 *Klebsiella* and *Pseudomonas* under the CTX treatment was also observed when different
174 incubation temperatures (30 °C and 40 °C instead of the 37 °C default) were tested
175 (Supplementary Fig. 5).
176
177 When mixed colonies were harvested and the relative abundances of the two species
178 were measured based on their colony forming unit (CFU) morphologies (Supplementary Fig. 4b),
179 we found that *Pseudomonas* dominated in cocultures with (99.7%) or without (99.9%) CTX
180 treatment (Fig. 1d). Distributing the biomass in the mixed colonies with respect to these relative
181 abundances, we found that *Klebsiella* always suffered from the mixed inoculation, while

Pseudomonas benefited from it under the CTX treatment (Supplementary Fig. 4a, compare the colored bars with and without a grey frame).

To facilitate the analysis of the colony composition in a spatially resolved manner, we used fluorescence proteins to label the two species (*Pseudomonas*-YFP and *Klebsiella*-mCherry). In a coculture consisting of these two labeled strains, we observed that *Klebsiella* was mostly confined at the seeding position, whereas the expanded colony front largely consisted of *Pseudomonas* (Supplementary Fig. 6).

Collectively, our results indicate that the CTX treatment suppressed *Pseudomonas*' spatial expansion, which was rescued by *Klebsiella* in a co-culture (Fig. 1c,d). In turn, the activated expansion of *Pseudomonas* suppressed the growth of *Klebsiella* (Fig. 1d; Supplementary Fig. 4a), which could be explained by a greater tolerance of *Pseudomonas* to CTX than *Klebsiella* (Fig. 1a).

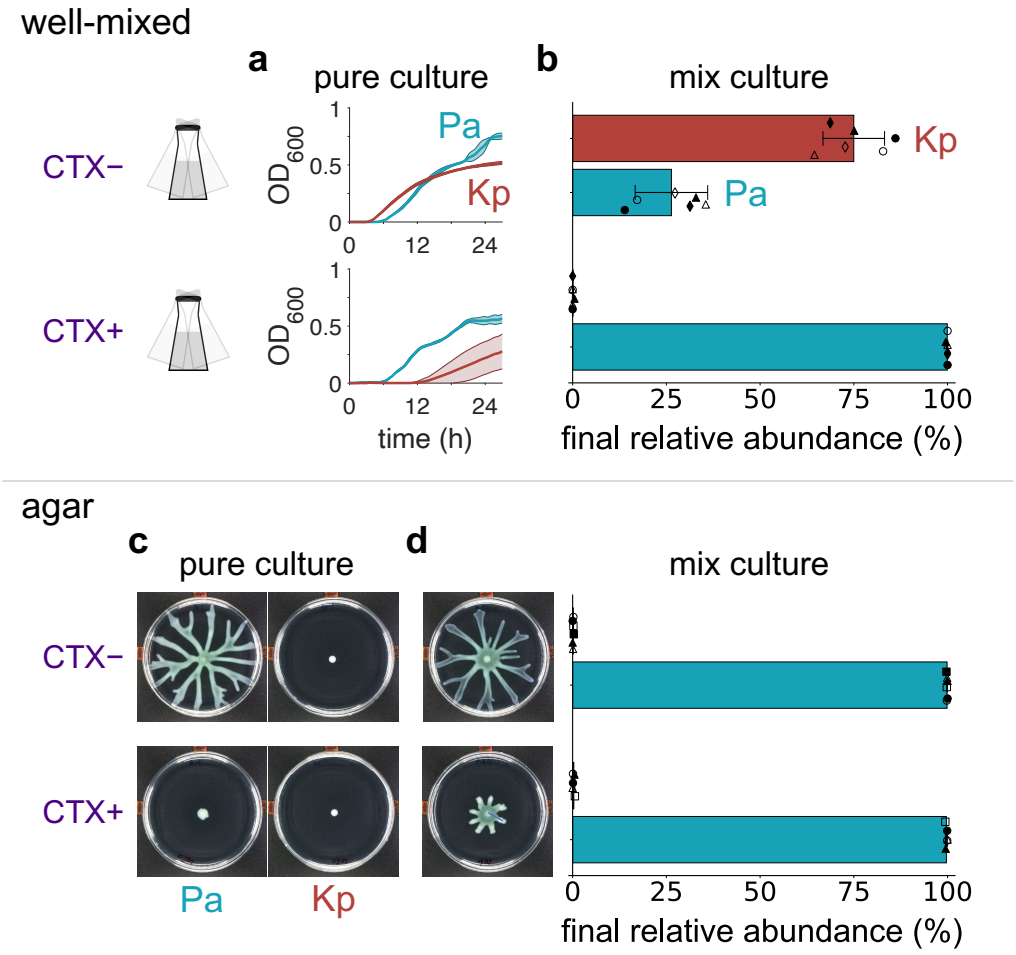

198

199 **Figure 1: *Klebsiella* and *Pseudomonas* exhibited collective range expansion under**
200 **CTX treatment at the cost of *Klebsiella*'s growth.** *Klebsiella* and *Pseudomonas* pure
201 cultures were grown overnight in lysogeny broth (LB). The cultures were then centrifuged,
202 and the resulting cell pellets were resuspended in phosphate-buffered saline (PBS)
203 supplemented with 8 g/l of casamino acids (see Methods). Kp: *Klebsiella*, Pa:
204 *Pseudomonas*.

205 **a. *Pseudomonas* tolerated CTX treatment better than *Klebsiella*.** *Well-mixed* pure
206 cultures of *Klebsiella* (dark red) and *Pseudomonas* (cyan) were inoculated at an initial
207 OD_{600} = ~ 2.1×10^{-5} (estimated based on dilutions applied to a cell suspension with
208 OD_{600} > 0.05) and without or with CTX (2.5 μg/ml) (top and bottom, respectively).
209 Curves and shades represent the average and the standard deviation, respectively,
210 from two biological replicates each with three technical replicates. See Methods for
211 details.

212 **b. *Pseudomonas* dominated *Klebsiella* under the CTX treatment in well-mixed co-**
213 **cultures.** Experiments were performed similarly to that in Fig. 1a. The liquid growth
214 media was inoculated with a 1:1 volume mixture of the two species at an initial OD_{600}
215 = ~ 2.1×10^{-5}. Co-cultures were incubated for 27 h and then harvested to measure
216 relative abundances by plating (Supplementary Fig. 4b). Circles, triangles, and
217 diamonds represent independent replicates whose technical replicates were shown by
218 solid or open markers. Data represented by diamonds were obtained using
219 fluorescently labeled strains (*Pseudomonas*-YFP and *Klebsiella*-mCherry). Data and
220 error bars represent the mean and the standard deviation from the independent
221 experiments after their technical replicates were averaged. When grown as a well-
222 mixed pure culture, each species produced less biomass in medium conditioned by
223 the other species than in unconditioned medium, demonstrating competition between
224 the two species (Supplementary Fig. 2).

225 **c. *Pseudomonas* range expansion was suppressed by CTX and rescued by**
226 ***Klebsiella*.** 20 ml of swarming agar (0.55 %) media surface was center inoculated with
227 1 μl of a 1:1 volume mixture of *Klebsiella* and *Pseudomonas* (OD_{600} = ~ 0.43). Colony
228 images were captured at 24 h, processed, analyzed for colony areas using a custom
229 Python script (Methods; Supplementary Fig. 3). Standard 100-mm petri dishes were

230 used. The images were equally adjusted for brightness and contrast for presentation.
231 See Supplementary Fig. 7 for raw images from all replicates.

232 **d. The rescue of the coculture range expansion occurred at the expense of**
233 ***Klebsiella*'s growth.** After being imaged at 24 h, whole colonies were harvested by
234 flooding with 5 ml of saline. The relative abundances of the two species in the harvests
235 were estimated based on their distinct CFU morphologies (Supplementary Fig. 4b).
236 Circles, triangles, and squares show independent experiments, for which the solid and
237 open markers represent technical replicates. The data and error bars represent the
238 mean and the standard deviation from the independent experiments after their
239 technical replicates were averaged. Standard 100-mm petri dishes were used. The
240 images were equally adjusted for brightness and contrast for presentation. See
241 Supplementary Fig. 7 for raw images from all replicates. Also, see Supplementary Fig.
242 4a for the total biomasses of the cell harvests as well as its distribution between
243 *Klebsiella* and *Pseudomonas*, estimated based on their relative abundances.

244

245 The rescuing by *Klebsiella* was likely due to its ability to produce Bla, which degrades
246 CTX[45] (Supplementary Table 1). To test this notion, we collected supernatants from the *Klebsiella*
247 pure cultures at ~ 6.3 h or media without cell inoculation as unconditioned control. After filter
248 sterilizing the supernatants, we tested whether CTX-sensitive *Escherichia coli* could grow in them
249 (Supplementary Fig. 8a, top). Following 21 h of incubation, *E.* coli exhibited detectable growth in
250 the *Klebsiella*-supernatant but not in the unconditioned control, consistent with the CTX
251 degradation by *Klebsiella*-produced Bla[45] (Supplementary Fig. 8a, bottom; see Supplementary
252 Fig. 8b, top for *Klebsiella* growth curves with the initial cell density of OD_{600} = ~ 5×10^{-4}, which was
253 used for this experiment).

254

255 **CTX suppressed *Pseudomonas*' spatial expansion in a dose-dependent manner.**

256 We next measured the suppression of *Pseudomonas* spatial expansion (in terms of
257 colonized area) using varied initial doses of CTX (0 to 2.5 μg/ml) (Supplementary Fig. 9). The
258 suppression increased with the initial CTX dose (A_0), approximately following a Hill inhibition
259 function.

260

261 *Pseudomonas* growth was virtually unaffected by CTX (2.5 μg/ml) treatment (Fig. 1a).
262 Thus, the suppression in *Pseudomonas*' spatial expansion (Fig. 1c; Supplementary Fig. 9) was
263 likely due to the loss of motility and correlated with filamentous cell morphology (Supplementary
264 Fig. 10), consistent with previous reports associating β-lactam-induced cell filamentation with

reduced motility[55,56]. The extent of the filamentation of *Pseudomonas* cells was reduced when inoculated in a mixture with *Klebsiella* (Supplementary Fig. 10), which restored *Pseudomonas*' spatial expansion (Fig. 1d). A similar filamentation of *Pseudomonas* was observed in well-mixed liquid cultures under CTX (2.5 μg/ml) treatment, with or without *Klebsiella* (Supplementary Fig. 11). The spatial expansion of *Pseudomonas* was eventually stopped by the antibiotic concentration far (1.5 ~ 2 cm) away from the inoculation point. This is because *Klebsiella* did not move along with *Pseudomonas* (Supplementary Fig. 6) and, hence, could no longer reduce the antibiotics to an ineffective concentration. Likewise, actively swarming *Pseudomonas* still needed *Klebsiella* for swarming when inoculated on fresh antibiotic media at ~ 4-times greater cell density than the original inoculum (Supplementary Fig. 12).

Theory reveals key determinants of the keystone engineering effect.

We conducted theoretical analysis to gain insight into the *Klebsiella*-mediated collective range expansion during antibiotic treatment. We assumed that the *Klebsiella* population leads to an antibiotic 'sink' and the growth media serves as a 'source' for antibiotics (Fig. 2a, top)[57]. The terms 'sink' and 'source' were inspired by the 'infinite source & point sink' reaction-diffusion framework we adapted below. We described the dependence of the effective spatial expansion ability (*M*) of *Pseudomonas* on the antibiotic concentration using the experimentally determined Hill function (Supplementary Fig. 9). Solving the system assuming cylindrical symmetry (see Supplementary Information for details), we have:

$$M = \frac{1}{1+a_0{}^h\left(\frac{\ln\left(d/_R\right)}{\ln\left(S/_R\right)}\right)^h} \qquad (1)$$

where $R > 0$ is the boundary of the 'sink' created by the *Klebsiella* population, $S \geq R$ is the domain boundary, $d \in [R, S]$ defines the distance of *Pseudomonas* from the 'sink' boundary, and $a_0 \in [0, \infty]$ is the initial antibiotic concentration normalized by its value for the half-maximum of *Pseudomonas*' effective spatial expansion ability ($a_0 = \frac{A_0}{A_C}$; see Supplementary Fig. 9 caption for A_C and h). Here, the 'sink' boundary *R* defines the radius of a circular 'clear zone' within which the antibiotic concentration is an ineffective lower boundary value. For the latter, we considered zero concentration for simplicity, though our theoretical framework can be applied to any arbitrary value. That is, each point on the 'clear zone' boundary acts as a 'point sink' for the antibiotics.

Note that we expect the 'clear zone' radius, R, to have two contributions: it scales with the physical size of the *Klebsiella* inoculum and has an additional term that increases nearly linearly with the characteristic diffusion length scale of Bla. This additional contribution is anticipated to depend only weakly on the *Klebsiella* seeding cell density (see Supplementary Information, Equation S7 for details).

For a constant d, M decreases from 1 and approaches 0 with increasing a_0. For a given a_0, M decreases with increasing d (Fig. 2a, bottom). For a sufficiently large a_0, *Pseudomonas*' effective spatial expansion ability is sharply activated when $d < L_K$, where L_K denotes the distance at which M is half-maximum. Thus, L_K is a measure of the spatial scale of keystone engineering. Critically, L_K can be substantially larger than R, indicating a long-range interaction (Fig. 2a, bottom, $L_K = \sim 3.2R$ for $a_0 = 2$).

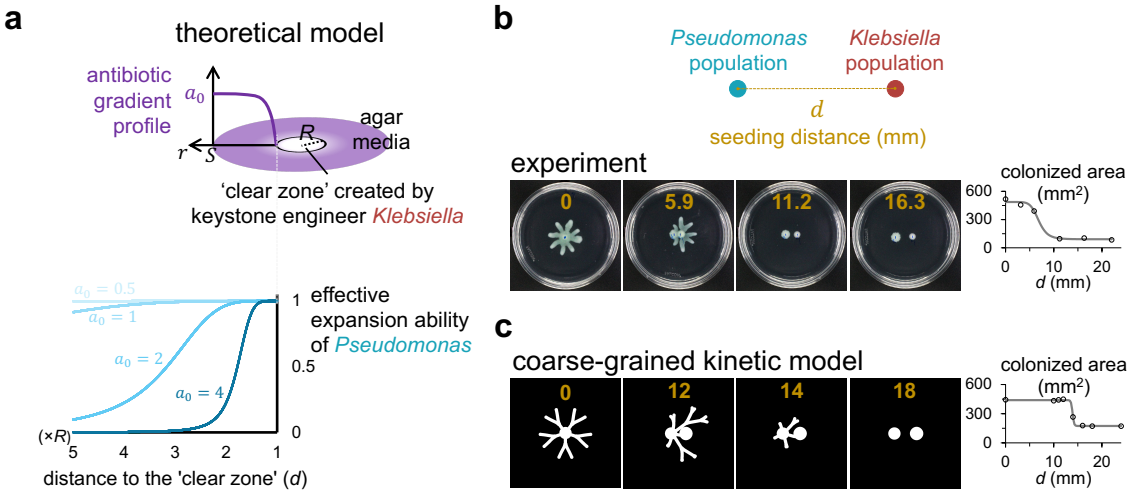

Figure 2: Spatial scale of the keystone engineering role.

a. Theoretical model:

***Top*: '*Klebsiella*–antibiotic' interaction**. Antibiotic concentration (a) has a steady-state gradient, under the assumption that a population of the keystone engineer *Klebsiella* acts as an antibiotic sink creating a 'clear zone' and the growth media serves as an infinite antibiotic source. a is smaller when closer to the 'sink', where the antibiotic concentration is minimized at an ineffective value (zero for simplicity; see Supplementary Information for details).

320 ***Bottom*: '*Klebsiella*-antibiotic-*Pseudomonas*' interactions.** Equation 1 predicts
321 that *Pseudomonas*' effective spatial expansion ability (*M*) is determined by its distance
322 to the sink boundary (*d*) and the initial antibiotic concentration (a_0). *h* = 6.642
323 (Supplementary Fig. 9), and *S*/*R* = 10 was assumed.

324 **b. Experiments corroborated the dependence of *Pseudomonas*' effective spatial**
325 **expansion ability on its distance to *Klebsiella.*** The experiment in Fig. 1d with CTX
326 (2.5 μg/ml) was repeated with the only difference being 1 μl from the *Pseudomonas*
327 (left) and 1 μl from the *Klebsiella* (right) cell suspensions were inoculated side-by-side
328 with various distance between them (gold in mm). The dishes were imaged at 23 h.
329 The colonized areas were measured using a custom Python script and manually
330 corrected using ImageJ when needed. The data was fitted to a Hill inhibition function
331 (solid curve), where the Hill coefficient and the spatial scale of the keystone
332 engineering (L_K) are 7.62 and 6.90 mm, respectively (R^2= 0.990). Each population
333 initially occupied a circular area with a radius of ~ 1.5 mm. Standard 100-mm petri
334 dishes were used. The images were equally adjusted for brightness and contrast for
335 presentation. See Supplementary Fig. 13 for the raw data from all replicates and
336 Supplementary Fig. 14 for the data from an experiment with the fluorescently labeled
337 strains. Note that the half-maximum suppressing CTX dose was 1.29 μg/ml
338 (Supplementary Fig. 9).

339 **c. A coarse-grained kinetic model recapitulated the experimental range expansion**
340 **patterns.** The results from the coarse-grained simulation at 48 h. *Left*. Black and white
341 indicates bacteria are absent and present, respectively. *Right*. Total area where
342 bacteria present was calculated using a custom MATLAB script and plotted as
343 colonized area as a function of the seeding distance (center-to-center) between the
344 *Pseudomonas* and *Klebsiella* populations (gold in mm). The data was again
345 approximated by a Hill inhibition function (solid curve), where the Hill coefficient and
346 L_K are 92.4 and 13.9 mm, respectively (R^2= 0.999). Each population initially occupied
347 a circular area with a radius of 5 mm. See Supplementary Fig. 15 for the data at
348 different time points. See Supplementary Table 2 for model parameters and initial
349 conditions.

350
351
352 **Experiments corroborated the theoretical predictions.**

353 To test Equation 1, we inoculated one *Klebsiella* population and one *Pseudomonas*
354 population at varied distance (d) under CTX (2.5 μg/ml) treatment. Then, we quantified the range
355 expansion as the colonized areas at 23 h, observing a sharp change at a certain distance value
356 (Fig. 2b), consistent with the prediction of the spatial scale of the keystone engineering (L_K) above.
357 The range expansion had a bias towards the *Klebsiella* population, which we confirmed by
358 repeating this experiment with the fluorescently labeled strains (Supplementary Fig. 14). We
359 demonstrated the robustness of the existence of L_K, repeating the same experiment, also with
360 varied *Klebsiella* seeding cell density (Supplementary Fig. 13).
361
362 **A coarse-grained kinetic model recapitulated the experimental range expansion patterns.**
363 The spatial patterns of the range expansion (Fig. 2b) were not considered in our theoretical
364 estimation of M and L_K above. The spatial patterns are a function of not only the antibiotic gradient
365 and the *Pseudomonas*' spatial expansion ability—which the antibiotic gradient determines—but
366 also the spatiotemporal dynamics of species and nutrient abundances. Thus, we next accounted
367 for these factors and built a coarse-grained model, enabling a more constrained simulation of
368 spatial expansion dynamics (Methods and Supplementary Table 2).
369
370 This model builds upon our previous models for *Pseudomonas* branching[58] and Bla-
371 mediated population dynamics in response to β-lactam treatment[45] (see Methods). We simulated
372 the range-expansion dynamics with varied seeding distance (d) between one *Klebsiella*
373 population and one *Pseudomonas* population. Again, we quantified the total colonized area (at
374 48 h; see Supplementary Fig. 15 for different time points) and found a sharp onset of range
375 expansion as d decreased below a critical value, consistent with the existence of L_K (Fig. 2c).
376 Simulations mimicking an intracellular degradation of antibiotics by an immotile species (zero
377 dispersal for the antibiotic-degrading enzyme and the species that produces it) yielded similar
378 results, suggesting that the 'antibiotic sink' role could be fulfilled without released public goods
379 (Supplementary Fig. 16).
380
381 **The keystone engineering occurred in a pairwise community of hospital sink co-isolates,**
382 ***Bacillus paranthracis* and *Pseudomonas aeruginosa*.**
383 Colonization of hospital sink drains (e.g., p-traps) has been associated with pathogens
384 such as *K. pneumoniae*[59] and *P. aeruginosa*[60]. Moreover, biofilms formed in the p-traps of
385 connected sinks and expanded upwards 2.5 cm/day, possibly due to surface-associated bacterial

386 motility[61]. If sufficiently close to the sink strainer, running sink water can lead to the spread of
387 bacteria to the environment[61], posing a health risk.
388
389 We next tested whether the keystone engineering could occur in communities of bacteria
390 isolated from the same sink p-trap at Duke University Hospital. Two isolates, 192621 and 192622,
391 were identified by 16S rDNA sequencing as *Bacillus paranthracis* and *P. aeruginosa*, respectively.
392
393 We first tested the effect of carbenicillin (CB; 10 μg/ml) treatment on the growth of the two
394 isolates. Specifically, we grew *B. paranthracis* 192621 (Bp) and *P. aeruginosa* 192622 (Pa22) in
395 pure liquid cultures without or with CB (10 μg/ml) (Fig. 3a). Both species tolerated the CB
396 treatment, but Pa22 grew faster than Bp under both conditions. When grown as a well-mixed pure
397 culture, each species produced less biomass in medium conditioned by the other species than in
398 unconditioned medium, demonstrating competition between the two species (Supplementary Fig.
399 17). If the two species primarily interact through competition in well-mixed cocultures, we expect
400 the dominance of Pa22 under both conditions. To this end, we tested the growth of mix cultures,
401 each starting with equal fractions of Bp and Pa22, with or without CB treatment. Indeed, Pa22
402 dominated after 27 h for both cases, where Bp was undetectable (< 0.1%) (Fig. 3b).
403
404 When tested on agar, however, only a mixture of Bp and Pa22 exhibited spatial expansion
405 after 24 h under treatment by CB (10 μg/ml; ~ 2.4-times the concentration for the half-maximum
406 suppression of the spatial expansion of Pa22 when alone, Supplementary Fig. 18) (Fig. 3c,d).
407 The mixture's spatial expansion under the CB treatment was maintained at 30 °C but was not at
408 40 °C (Supplementary Fig. 19), indicating the context-dependence of mechanism. While mixing
409 Pa22 with Bp promoted biomass production under the CB treatment by 4-fold, Bp itself became
410 undetectable (< 0.1%) in the final population (Fig. 3d; see Supplementary Fig. 20 for biomass
411 data). Supernatants from CB-treated pure cultures of Bp allowed the growth of CB-sensitive *E.*
412 *coli* (Supplementary Fig. 21), indicating the degradation of CB in the environment by Bp. These
413 results suggest that Bp served the keystone engineer role on Pa22 only during community spatial
414 expansion by degrading the antibiotics in the environment.
415
416 The principles we uncovered from the pairwise communities above (Fig. 1,2,3) are likely
417 generalizable: When we used a variant of the CB-sensitive *E. coli*, which was engineered to
418 express Bla conferring CB resistance[62,63], it also rescued *Pseudomonas* swarming from CB
419 inhibition (Supplementary Fig. 22).

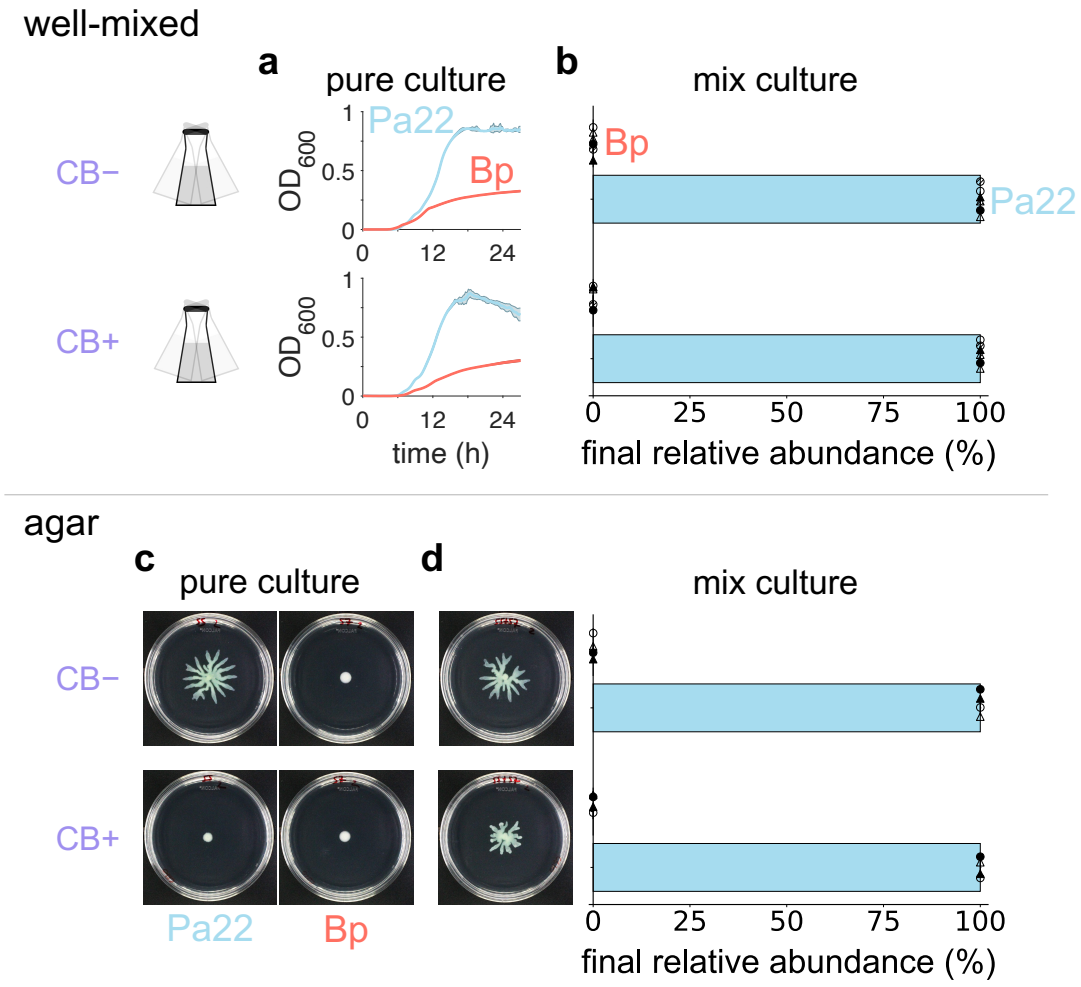

Figure 3: The keystone engineering in a pairwise community of hospital sink isolates, Bp and Pa22. Bp and Pa22 pure cultures were grown overnight in LB. The cultures were then centrifuged, and the resulting cell pellets were resuspended in PBS supplemented with 8 g/l of casamino acids (see Methods). Bp: *Bacillus paranthracis*, Pa22: *Pseudomonas aeruginosa* 192622.

a. Pa22 tolerated CB treatment better than Bp. *Well-mixed* cultures of Bp (red) and Pa22 (light blue) were inoculated, with the initial cell density of OD_{600} = ~ 2.1×10^{-5} (estimated based on dilutions applied to a cell suspension with OD_{600} > 0.05), and without or with CB (10 μg/ml) (top and bottom, respectively). Curves and shades represent the average and the standard deviation, respectively, from two biological replicates each with three technical replicates.

434 b. **Pa22 dominated Bp in well-mixed cocultures via competition.** The liquid growth
435 media was inoculated with a 1:1 volume mixture of the two species at the starting cell
436 density of OD_{600} = ~ 2.1×10^{-5}. Co-cultures were incubated for 27 h and then harvested
437 to measure relative abundances by plating (Supplementary Fig. 20b). Circles and
438 triangles represent independent replicates whose technical replicates were shown by
439 solid, open, or lined markers. Data and error bars represent the mean and the standard
440 deviation from the independent experiments after their technical replicates were
441 averaged. When grown as a well-mixed pure culture, each species produced less
442 biomass in medium conditioned by the other species than in unconditioned medium,
443 demonstrating competition between the two species (Supplementary Fig. 17).
444 c. **Pa22's range expansion was suppressed by CB treatment and rescued by Bp.**
445 20 ml of agar (0.55 %) media surface was center inoculated with 1 μl of a 1:1 volume
446 mixture of Bp and Pa22 with or without CB (10 μg/ml) at the initial cell density of OD_{600}
447 = ~ 0.34 or ~ 0.43). Images of the colonies were captured at 24 h. The images were
448 processed and analyzed for colonized areas using a custom Python script (Methods).
449 Standard 100-mm petri dishes were used. The images were equally adjusted for
450 brightness and contrast for presentation. See Supplementary Fig. 23 or all raw images.
451 d. **The rescue of the coculture range expansion occurred at the expense of Bp's**
452 **growth.** After being imaged at 24 h, whole colonies were harvested by flooding with 5
453 ml of saline. The total biomass was calculated by multiplying the absorbance (OD_{600})
454 and the volume of the suspension. The relative abundances of the two species in the
455 harvests were estimated based on their distinct CFU morphologies (Supplementary
456 Fig. 20b). Circles (inoculum density of OD_{600} = ~ 0.43) and triangles (inoculum density
457 of OD_{600} = ~ 0.34) represent independent experiments, for which the solid and open
458 markers show technical replicates. Data and error bars show the mean and standard
459 deviation, respectively, from all the replicates. Standard 100-mm petri dishes were
460 used. The images were equally adjusted for brightness and contrast for presentation.
461 See Supplementary Fig. 23 or all raw images. Also, see Supplementary Fig. 20a for
462 the total biomasses of the cell harvests as well as its distribution between Bp and
463 Pa22, estimated based on their relative abundances.
464
465 **Keystone engineering occurred in a synthetic community of sink isolates.**
466 Pairwise communities above enabled us to investigate mechanistic underpinnings of the
467 keystone engineering that enables collective range expansion under antibiotic treatment. To

468 evaluate the generalizability of the mechanism, we next tested if Bp's keystone engineering on
469 Pa22's spatial expansion could occur in the presence of other members of sink isolates. To this
470 end, we assembled an eight-member community, which we termed 'SynkC', by introducing six
471 additional isolates from the same sink sample from which we isolated both Bp and Pa22. SynkC
472 consists of six distinct taxonomic groups based on 16S rDNA-based microbiome sequencing.
473 Seven out of the eight SynkC members are genotypically and/or phenotypically distinct
474 (Supplementary Fig. 24). In addition to Pa22, only one other SynkC member showed spatial
475 expansion ability on its own (Supplementary Fig. 24a, *Bacillus sp.* ESY92). When tested alone,
476 two SynkC members did not tolerate the CB treatment, and the others exhibited various degrees
477 of tolerance (Supplementary Fig. 24b).
478
479 Whole genome sequencing of the SynkC members revealed that each member had at
480 least one Bla gene. Bp had the most (17) Bla genes followed by Pa22 (7), while Bp was the only
481 isolate carrying a class A Bla, according to Ambler's classification scheme, based on amino acid
482 sequence similarities of known Bla proteins (Supplementary Table 1). These sequencing results
483 suggest a greater or a unique potential of Bp to degrade certain β-lactam antibiotics. Accordingly,
484 in pairwise cultures, Bp was the only one that rescued the Pa22 spatial expansion from the CB
485 treatment inhibition (Supplementary Fig. 25).
486
487 We ran agar experiments with SynkC with equal starting biomasses of all the eight
488 members or by leaving out Bp (SynkC-Bp). Again, spatial expansion under the CB treatment
489 occurred only when Bp was included (Fig. 4, images), though Bp was not detected in the final
490 population of SynkC (Fig. 4, pie charts). In addition to promoting the spatial expansion and ~ 2.7-
491 fold greater total biomass, the initial presence of Bp also increased community diversity under the
492 CB treatment. Specifically, while only Pa22 was detected at the end of the SynkC-Bp experiment,
493 both Pa22 and *Enterobacter sp*. were detected in the final SynkC community (Fig. 4, pie charts).
494 This suggests that *Enterobacter sp.* should also be considered when analyzing the precise spatial
495 distribution of bacteria. However, *Enterobacter sp.* cannot spread alone (Supplementary Fig.
496 24a), so any spatial of *Enterobacter sp*. must depend on other species such as Pa22.
497

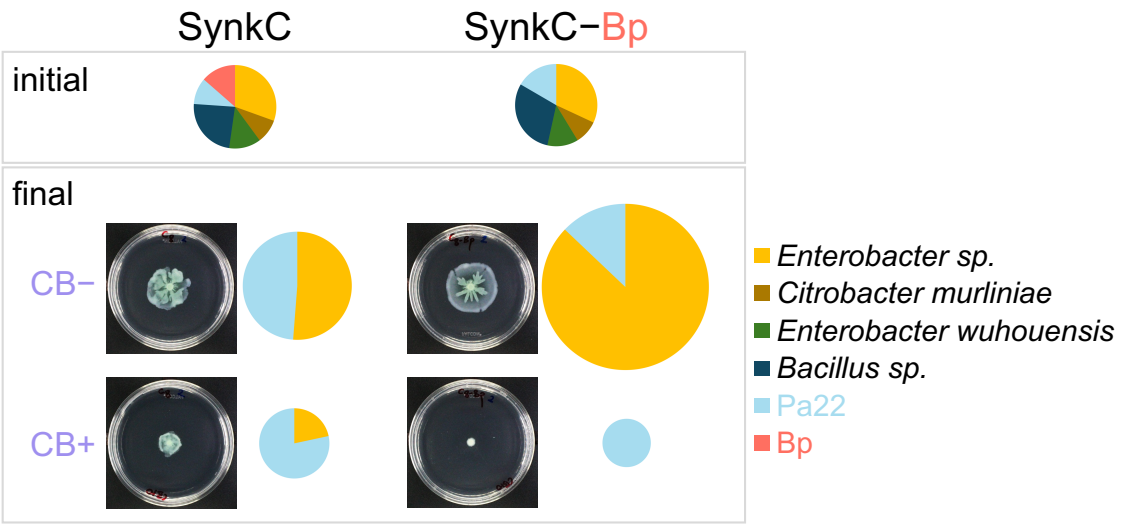

Figure 4: The keystone engineering in SynkC, an 8-member, synthetic community of hospital sink co-isolates.

The agar (0.55%) surface was inoculated with 1 μl of a mixture containing equal biomasses of all the eight isolates (SynkC) or all but Bp (SynkC–Bp) (OD_{600} = ~ 0.34). Images of the colonies were captured at 24 h. Then, whole colonies were harvested by flooding with ~ 5 ml of saline. The biomasses of the cell harvests were calculated by measuring the absorbance (OD_{600}) of each harvest suspension and multiplying it by the suspension volume. The initial and final cell suspensions were stored as frozen glycerol stocks and underwent 16S microbiome sequencing to determine the initial and final relative abundances of different community members (a 0.5 % cut-off value applied). Each of the pie charts above shows six groups, with the *Enterobacter sp.* and *Bacillus sp.* groups representing the combined abundance of two isolates each, while all other groups represent a single isolate. For the final time point, relative areas of the pie charts represent the distribution of the respective biomasses measured. Two independent experiments, each with technical replicates, yielded similar results. A representative set of data was shown here, after the images were equally processed for brightness and contrast for presentation. Standard 100-mm petri dishes were used. CB (10 μg/ml) was used when applicable. See Supplementary Fig. 26 for the raw data from all replicates. See Supplementary Fig. 24 for the identities and phenotypes of the individual isolates.

Discussion

523 Our study provides a concrete demonstration that context—specifically spatial structure
524 and chemical stress—can reveal a species' keystone engineer role. By degrading β-lactam
525 antibiotics, an immotile Bla-producing species (*K. pneumoniae* or *Bacillus paranthracis*) creates
526 a 'clear zone' that restores the motility-based range expansion of a more resilient partner (*P.*
527 *aeruginosa*). The keystone engineering we report here represents a form of facilitation. *K.*
528 *pneumoniae* and *B. paranthracis* actively modify the environment by degrading antibiotics,
529 thereby enabling the range expansion of *P. aeruginosa*. However, this facilitation is at the cost of
530 the facilitators themselves—driving them to an extreme minority population, apparently through
531 competitive exclusion by *P. aeruginosa*. Although the keystone engineer eventually becomes a
532 minority due to competition, its transient facilitation is essential for spatial expansion and overall
533 community success. This mechanism could contribute to the observed rapid biofilm formation in
534 sink-associated microbial communities[61].
535
536 Our results broaden the canonical interpretation of keystone species, which typically
537 emphasizes effects on growth or community structure[14-17,24,28-33]. Two contextual factors are
538 critical for our system. One is spatial expansion, as mobility only matters in a spatially structured
539 environment. This context-dependency is reminiscent of a recent example in which we show that
540 the spatial expansion of *Pseudomonas* not only makes a cooperative trait essential[42] but also
541 allows non-cooperating variants (so-called "cheaters") to leverage their growth advantage from
542 the lack of cooperative trait expression, enabling them to outcompete the cooperating
543 individuals[43]. The other contextual factor is antibiotic stress, which primarily suppresses mobility
544 instead of the growth of *Pseudomonas*. Together, these factors shift the net effect of the keystone
545 engineer from competitive to facilitative. This shift aligns with the stress gradient hypothesis,
546 which suggests that positive interactions dominate negative interactions in more stressful
547 environments[64-67].
548
549 The principles uncovered here are likely generalizable. Other species or consortia could
550 similarly modify their environment—through pH shifts[24], enzyme secretion[68,69], nutrient
551 release/break-down[31,68,69], or other chemical changes—to unlock traits like motility[70,71], biofilm
552 growth[72-74], or nutrient utilization (i.e., necrotrophy[68]) relevant only in spatially structured habitats.
553 Such facilitation may be common in natural and engineered microbial communities but remain
554 untapped due to a lack of spatially explicit experimental inquiry.
555

556 Clinically, consistent with the notion of private versus public benefits of Bla producers in
557 bacterial communities[75], our work suggests that certain Bla producers may play a crucial, even if
558 transient, role in promoting the spread of more virulent pathogens, such as *Pseudomonas*, even
559 if they remain undetected in standard assays. Current microbiome analyses often exclude low-
560 abundance taxa[76], potentially missing these keystone engineers and underestimating their
561 influence on infection dynamics.
562
563 In conclusion, recognizing the context-dependent emergence of keystone engineering
564 enriches our understanding of microbial ecology, offers insights for controlling infections, and
565 opens new avenues for studying hidden facilitators in complex microbial ecosystems.
566
567 **Methods**
568
569 **Bacterial growth media and procedures**

570 In every experiment, bacteria were first streaked on a lysogeny broth (LB) agar plate from
571 their frozen glycerol stock, and a single colony was incubated overnight in liquid LB media at 37
572 °C and 225 r.p.m.
573
574 For all experiments, PBS (2.4 g/l Na_2HPO_4 (anhydrous), 3 g/l KH_2PO_4 (anhydrous), 0.5 g/l
575 NaCl, 1 mM $MgSO_4$, and 0.1 mM $CaCl_2$) supplemented with casamino acids (8 g/l, unless
576 otherwise noted) was used. Agar (final concentration of 0.55 %) was used when applicable.
577
578 The media was prepared following a recipe adapted from Xavier *et al*.[77]: To make 1 liter
579 of 5x phosphate buffer stock solution, 12 g Na_2HPO_4 (anhydrous), 15 g KH_2PO_4 (anhydrous), and
580 2.5 g NaCl were dissolved in deionized water and sterilized by autoclaving. The casamino acids
581 stock solutions were made at 20 % (w/v) by microwaving 40 g casamino acids (Gibco™ Bacto™
582 223120) in deionized water, sterilized by filtering (0.22 μm) and stored at 4 °C. The main solutions
583 of agar were made at 1.25 % (w/v) on the day of the experiment dissolving granulated agar (BD
584 Difco™ 214530) in deionized water and sterilizing by autoclaving. Then, appropriate amounts
585 were immediately used to prepare the experimental media.
586
587 In the experiments and overnight cultures with the *Pseudomonas*-YFP and *Klebsiella*-
588 mCherry variants, gentamycin (15 μg/ml) was added for the maintenance of the plasmids. aTc

589 (100 ng/ml) was also added for inducing the mCherry expression. All antibiotic solutions used in
590 the study were made fresh on the day of the experiment.
591
592 All OD_{600} measurements were taken using 200 µl samples and a plate reader (Tecan
593 Infinite 200).
594
595 *Well-mixed liquid cultures*
596 We grew 2-3 ml cells in 16 ml culture tubes at 37 °C and 225 r.p.m. The cultures with aTc
597 were protected from light.
598
599 Growth curve experiments
600 We measured the growth curves of bacteria using a plate reader (Tecan Infinite 200). In
601 each well of a 96-well plate, we added 195 µl liquid media and 5 µl cell inoculum culture (prepared
602 by centrifuging overnight-grown cells at 1150 g for 5 min and then resuspending in the liquid
603 medium). To prevent evaporation, we used Nunc Edge multi-well plates (Thermo Scientific) with
604 built-in water reservoirs. In addition to the built-in water reservoirs, we also reserved all the edge
605 wells for water only. The cells were then incubated in the plate reader at 37 °C, and
606 OD_{600} measurements were taken at 10 min intervals after the plate being shaken rigorously. For
607 technical replicates of a particular condition, cells from the same inoculum were inoculated in
608 different wells of a 96-well plate and measured. Background signals measured from media
609 containing no cells were subtracted from the data. Custom MATLAB scripts were used for data
610 analysis, during which a four time point moving average was applied to the raw OD_{600} time series
611 data.
612
613 *Agar media experiments*
614 20 ml growth media was solidified in 100 mm petri dishes. Overnight-grown cells were
615 centrifuged at 1150 g for 5 min and then resuspended in the liquid medium to prepare a cell
616 inoculum culture. The seeding droplet volume from cell inoculum cultures was 1 µl. The seeded
617 plates were incubated at 37 °C, agar side up.
618
619 *CTX/CB environmental degradation assays*
620 The protocol used was adapted with minimal changes from our previous study[45]: Briefly,
621 3 ml liquid media with/without the keystone engineer bacteria (*Klebsiella* or Bp) inoculated (initial
622 cell density of OD_{600} = ~ 5×10^{-4}) and with/without the antibiotic (2.5 μg/ml CTX or 10 μg/ml CB)

623 addition were incubated at 37 °C and 225 r.p.m. At ~ 6.3 h, 1 ml samples from the media were
624 removed, in which clavulanic acid (5 µg/ml final concentration) was then added to prevent any
625 further Bla activity. Next, supernatants were prepared by filtration of these 1 ml samples using
626 0.22 μm cellulose acetate filters (VWR). Finally, the supernatants were inoculated with *E. coli*
627 MC4100Z1 at initial cell density of OD_{600} = ~ 5×10^{-4}, at which the *E. coli* is sensitive to the antibiotic
628 treatments here. Then, OD_{600} measurements were taken after 21 h incubation at 37 °C at 225
629 r.p.m.
630
631 *Spent media assays*
632 Similar to the "CTX/CB environmental degradation assays" above, 3 ml liquid culture
633 media were incubated for ~ 6.3 h at 37 °C and 225 r.p.m. with no inoculant (for an unconditioned
634 control media) or with *Klebsiella* or *Pseudomonas* (or with Bp or Pa22 at the initial cell densities
635 odf OD_{600} = ~ 5×10^{-4}). Then, supernatants were collected by filtration using 0.22 µm cellulose
636 acetate filters (VWR). Within each pairwise system, the filtered supernatants of each species were
637 cross-inoculated with the other species (OD_{600} = ~ 5×10^{-4}). Subsequently, growth curve
638 measurements were performed in a plate reader at 37 °C, as described above.
639
640 *Relative abundance measurements based on colony forming unit (CFU) morphology*
641 As shown in Supplementary Fig. 4b and Supplementary Fig. 20b, CFUs were grown on
642 LB agar (1.5 %) for 20 h at 37 °C to determine the relative abundance of the constituent species
643 in pairwise mixed cultures. To do so, cell harvests were serially diluted in sterile saline (11.6 g/l
644 NaCl) solution down to ~ 100 CFUs per 100 µl spread on a 100-mm LB agar plate.
645
646 **Bacterial strains**
647 *P. aeruginosa* PA14 (*Pseudomonas*), a clinical *K. pneumoniae* isolate D-005 from
648 Deverick J. Anderson's laboratory (*Klebsiella*), *E. coli* MC4100Z1, *E. coli* MC4100Z1 with a
649 plasmid that encodes an engineered cytoplasmic β-lactamase (*E. coli* Bla+)[62], and the hospital
650 sink p-trap isolates described below were used. For some experiments variant strains that
651 expressed spectrally distinct fluorescent proteins from a plasmid, *Pseudomonas*-YFP[43] and
652 *Klebsiella*-mCherry (this study, see Methods and Supplementary Table 3), were used.
653
654 *Construction of the Klebsiella-mCherry strain*
655 <u>Strain & transformation</u>

656 Zymo Mix & Go Transformation kit (Zymo Research) was used to make *K. pneumoniae*
657 D-005 chemically competent with one modification: the overnight culture of D-005 was re-grown
658 in super optimal broth (SOB) supplemented by 0.7 mM (final concentration)
659 ethylenediaminetetraacetic acid (EDTA)[78].
660
661 Plasmid construction
662 ptetmCherryGMR was constructed from the parent plasmids ptetmCherry[79], pUCP30T-
663 eCFP plasmid[80], and pJ1996_v2[81]. The ptetmCherry plasmid without the chloramphenicol
664 resistance gene, the gentamicin resistance gene, and a DNA fragment containing two
665 transcription terminators were PCR amplified from the ptetmCherry, pUCP30T-eCFP, and
666 pJ1996_v2 plasmids, respectively, by DNA primers with overhangs. The resulting linear DNA
667 fragments were digested by DpnI and subsequently column purified with DAN Clean & Concentor-
668 5 (Zymo Research). Then, they were ligated together with NEBuilder HiFi DNA Assembly Master
669 Mix (NEB #E2621) to yield the final plasmid. The final plasmid was transformed into Top10F' to
670 propagate, miniprepared with Zymo Plasmid Miniprep-Classic kit (Zymo Research) and
671 sequenced by Sanger sequencing (Genewiz/Azenta Life Sciences) to validate.
672
673 All the DNA primers were purchased from Integrated DNA Technologies and listed in
674 Supplementary Table 3.
675
676 *SynkC: Isolation of bacteria from the sink p-traps and their taxonomic identification*
677

Strain identity	**Taxonomic group name we used**	**Identity suggested by the Azenta Life Sciences pipeline**	**Identity suggested by the SeqCenter LLC pipeline**
ESY55	Pa22	*Pseudomonas aeruginosa* ATCC10145	*Pseudomonas aeruginosa*
ESY57	Bp	*Bacillus paranthracis* MCCC1A00395	*Bacillus*
ESY66	*Enterobacter wuhouensis*	*Enterobacter wuhouensis/ludwigii*	*Enterobacter cloacae*
ESY73	*Bacillus sp*.	*Bacillus aerophilus/stratosphericus/altitudinis*	*Bacillus sp*.

ESY80	*Citrobacter murliniae*	*Citrobacter murliniae* / *freundii*	*Citrobacter*
ESY83	*Enterobacter sp*.	*Enterobacter bugandensis* 247BMC	*Enterobacter*
ESY92	*Bacillus sp*.	*Bacillus aerophilus*/*stratosphericus*/*altitudinis*	*Bacillus sp*.
ESY93	*Enterobacter sp*.	*Enterobacter sichuanensis*/*asburiae*	*Enterobacter*

678

679 The members of SynkC were isolated by propagations of a sample collected from a sink
680 p-trap in an intensive care unit in a recently constructed bedtower at the Duke University Hospital.
681 Sterile tubing was fed down into the p-trap and a 50 ml syringe was used to agitate the fluid to
682 collect biofilm portions and then withdraw a sample[82]. 50 µl of p-trap water was used to inoculate
683 950 µl of tryptic soy broth in a 2 ml deep well plate (Thermo Scientific) and grown for 16 h at 37
684 °C with shaking at 700 r.p.m. The resulting culture was glycerol stocked (25% glycerol) and frozen.
685 In parallel, it was serially diluted to 10^{-6} in phosphate buffered saline and 10 µl of dilutions from
686 10^{-3} to 10^{-6} were plated on tryptic soy agar (TSA) with and without 100 µg/ml carbenicillin. The
687 plates were incubated at 37 °C for 10 h and at room temperature for 66 h.

688

689 Pa22 (ESY55) and Bp (ESY57) were isolated via restreaking different parts of the resulting
690 colonies on fresh agar plates and incubating for 18 h at 37 °C. A new set of overnight cultures
691 were then made by inoculating 2 ml of tryptic soy broth with individual colonies on the restreaked
692 plates and incubating for 16 hours at 37 °C. These cultures were then glycerol stocked as the
693 eventual Pa22 and Bp. Subsequent colonies from these stocks were sent for 16S sequencing at
694 Azenta Life Sciences for species identification.

695

696 ESY66 and ESY73 were isolated as follows: First, the glycerol stock of the original
697 overnight culture described above was inoculated LB and then grown for ~ 8 h at 37 °C with
698 shaking at 225 r.p.m. The resulting culture was glycerol stocked (25% glycerol) and frozen. This
699 stock is called the "master stock" hereafter. The master stock was diluted ~ 10^4 -fold in 11.6 g/l
700 saline, and 100 µl of the dilution was plated on TSA plates. The plates were incubated at 37 °C
701 for ~ 20 h. Individual colonies were restreaked on LB agar plates, and the plates were incubated
702 at 37 °C for ~ 20 h, again. Then, overnight cultures were grown by inoculating 2 ml of LB with
703 individual colonies from the restreaked plates and incubating for ~ 18 h at 37 °C with shaking at
704 225 r.p.m. These cultures were then glycerol stocked as the eventual isolates used in this study.

705 Individual colonies from these stocks were sent for 16S sequencing at Azenta Life Sciences for
706 species identification.
707
708 ESY80, ESY83, ESY92, and ESY93 were isolated as follows: First, ~ 1 μl from the master
709 stock was inoculated on swarming agar media and incubated for ~ 24 h at 37 °C. The final colony
710 was suspended in 11.6 g/l saline and then glycerol (25 %) stocked and frozen. This new frozen
711 stock was diluted ~ 10^5-fold in 11.6 g/l saline, and 100 μl of the dilution was plated on TSA plates.
712 The plates were incubated at 37 °C for ~ 20 h. Individual colonies were restreaked on LB agar
713 plates, and the plates were incubated at 37 °C for ~ 20 h, again. Then, overnight cultures were
714 grown by inoculating 2 ml of LB with individual colonies from the restreaked plates and incubating
715 for ~ 18 h at 37 °C with shaking at 225 r.p.m. These cultures were then glycerol stocked as the
716 eventual isolates used in this study. Individual colonies from these stocks were sent for 16S
717 sequencing at Azenta Life Sciences for species identification.
718
719 *16S microbiome sequencing by SeqCenter*
720 16S V3/V4 region sequencing (20000 reads) service of SeqCenter, LLC was used.
721 Aliquots from cell harvests were supplemented by glycerol (25 % final concentration) before being
722 frozen at -80 °C. The frozen aliquots were shipped overnight to the company's facility on dry ice.
723
724 DNA extraction
725 All standard DNA extractions at SeqCenter follow the ZymoBIOMICS™ DNA Miniprep Kit.
726 20 - 200 μl from the samples submitted were transferred into 550 μl of lysis solution. Cells
727 suspended in lysis solution were transferred into the ZR BashingBead™ Lysis Tubes and
728 mechanically lysed using the MP FastPrep-24™ lysis system with 1 min of lysis at maximum
729 speed and 5 min of rest for 5 cycles. Samples were then centrifuged at 10000 g for 1 min. 400 μl
730 of supernatant was transferred from the ZR BashingBead™ Lysis Tube to a Zymo-Spin™ III-F
731 Filter and centrifuged at 8000 g for 1 min. 1200 μl of ZymoBIOMICS™ DNA Binding Buffer was
732 added to the effluent and mixed via pipetting. 800 μl of this solution was transferred to a Zymo-
733 Spin™ IICR Column and centrifuged at 10000 g for 1 min. This step was repeated until all material
734 was loaded onto the Zymo-Spin™ IICR Column. DNA bound to the Zymo-Spin™ IICR Column
735 was washed 3 times with 400 μl and 700 μl of ZymoBIOMICS™ DNA Wash Buffer 1 and then
736 200 μl of ZymoBIOMICS™ DNA Wash Buffer 2 with a 1-min spin down at 10000 g for each,
737 respectively. Washed DNA was eluted using 75 μl of ZymoBIOMICS™ DNase/RNase Free Water
738 following a 5-min incubation at room temperature and a 1-min spin down at 10000 g. The Zymo-

739 Spin™ III-HRC Filter was prepared using 600 µl of the ZymoBIOMICS™ HRC Prep Solution and
740 a centrifugation at 8000 g for 3 min. Eluted DNA was then purified by running the effluent through
741 the prepared Zymo-Spin™ III-HRC Filter. Final DNA concentrations were determined via Qubit.
742
743 Sequencing
744 Samples were prepared using Zymo Research's Quick-16S kit with phased primers
745 targeting the V3/V4 regions of the 16S gene. The specific primer sequences are found below:
746

Amplified region	Forward sequence	Reverse sequence
V3/V4	341f CCTACGGGDGGCWGCAG CCTAYGGGGYGCWGCAG	806r GACTACNVGGGTMTCTAATCC

747
748 Following clean up and normalization, samples were sequenced on a P1 600cyc
749 NextSeq2000 Flowcell to generate 2×301 bp paired end (PE) reads. Quality control and adapter
750 trimming was performed with bcl-convert (v4.2.4).
751
752 Analysis
753 Sequences were imported to Qiime2[83] for analysis. Primer sequences were removed
754 using Qiime2's cutadapt[84] plugin using the following degenerate primer queries:
755

Region	Forward trim sequence	Reverse trim sequence
V3/V4	CCTAYGGGNBGCWGCAG	GACTACNVGGGTMTCTAATCC

756
757 Sequences were then denoised using Qiime2's dada2 plugin[85]. Denoised sequences were
758 assigned operational taxonomic units (OTUs) using the "Silva 138 99% OTUs full-length
759 sequence database" and the VSEARCH[86] utility within Qiime2's feature-classifier plugin. OTUs
760 were then collapsed to their lowest taxonomic units, and their counts were converted to reflect
761 their relative frequency within a sample.
762
763 Note that, for SynkC, neither the SeqCenter microbiome sequencing nor the Azenta Life
764 Sciences 16S sequencing-based species identification pipelines could distinguish the members
765 within the *Enterobacter sp*. and *Bacillus sp* taxonomic groups. The identities of Pa22, Bp,
766 *Citrobacter murliniae*, and *Enterobacter wuhouensis* were better resolved to species level from
767 the best fits of the Azenta Life Sciences pipeline, so we used those identities. We confirmed that

768 these four isolates did not fall into either the *Enterobacter sp*. or the *Bacillus sp.* taxonomic groups
769 in the SeqCenter pipeline, which was used to generate the relative abundance data in Fig. 4 and
770 Supplementary Fig. 26.
771
772 *Whole genome sequencing by SeqCenter LLC*
773 DNA extraction
774 DNA extractions were performed by SeqCenter LLC following the ZymoBIOMICS™ DNA
775 Miniprep Kit: A loopful of cells (~ 50 – 100 mg) were aseptically scraped from the submitted agar
776 plates and resuspended in 750 µl of lysis solution.
777
778 Cells suspended in lysis solution were transferred into the ZR BashingBead™ Lysis Tubes
779 and mechanically lysed using the MP FastPrep-24™ lysis system with 1 min of lysis at maximum
780 speed and 3 min of rest for 2 cycles. Samples were then centrifuged at 10,000 rcf for 1 min. 400
781 µl of supernatant was transferred from the ZR BashingBead™ Lysis Tube to a Zymo-Spin™ III-F
782 Filter and centrifuged at 8,000 rcf for 1 min. 1,200 µl of ZymoBIOMICS™ DNA Binding Buffer was
783 added to the effluent and mixed via pipetting. 800 µl of this solution was transferred to a Zymo-
784 Spin™ IICR Column and centrifuged at 10,000 rcf for 1 min. This step was repeated until all
785 material was loaded onto the Zymo-Spin™ IICR Column.
786
787 DNA bound to the Zymo-Spin™ IICR Column was washed 3 times with 400 µl and 700 µl
788 of ZymoBIOMICS™ DNA Wash Buffer 1 and then 200 µl of ZymoBIOMICS™ DNA Wash Buffer
789 2 with a 1-min spin down at 10,000 rcf for each, respectively. Washed DNA was eluted using 75
790 µl of ZymoBIOMICS™ DNase/RNase Free Water following a 5-min incubation at room
791 temperature and a 1-min spin down at 10,000 rcf. The Zymo-Spin™ III-HRC Filter was prepared
792 using 600 µl of the ZymoBIOMICS™ HRC Prep Solution and a centrifugation at 8,000 rcf for 3
793 min. Eluted DNA was then purified by running the effluent through the prepared Zymo-Spin™ III-
794 HRC Filter. Final DNA concentrations were determined via Qubit.
795
796 Illumina sequencing
797 Illumina sequencing libraries were prepared using the tagmentation-based and PCR-
798 based Illumina DNA Prep kit and custom Integrated DNA Technologies 10 bp unique dual indices
799 with a target insert size of 280 bp. No additional DNA fragmentation or size selection steps were
800 performed. Illumina sequencing was performed on an Illumina NovaSeq X Plus sequencer in one
801 or more multiplexed shared-flow-cell runs, producing 2×151 bp paired-end reads. Demultiplexing,

802 quality control and adapter trimming was performed with bcl-convert (a proprietary Illumina
803 software for the conversion of bcl files to basecalls, v4.2.4).
804
805 Illumina short-read assembly and annotation
806 Short read assembly was performed with Unicycler[87]. Assembly statistics were recorded
807 with QUAST[88]. Samples were annotated with Bakta[89].
808

Tool	Version	Parameters
unicycler	0.5.0	default parameters
quast	5.2.0	default parameters
bakta	1.8.1	default parameters; db version 5.0

809
810 **Imaging**
811 Bacterial colonies on agar plates were imaged with a UVP Colony Doc-It Imaging Station
812 with epi white light, using the same brightness and contrast settings for all images. The same z-
813 plane focus was applied to all images within the same independent experiment.
814
815 Microscopic imaging was performed using a Keyence BZ-X710 microscope and Keyence
816 BZX Software Suite 1.3.1.1. To image a whole swarming colony, its entire plate was scanned and
817 imaged, and the resulting images were stitched using the built-in algorithm of the software.
818
819 **Image analyses**
820 A custom Python script was used for processing and analyzing the colonized area for
821 bacterial colony images. This script firsts finds and removes the plate boundaries. Then, the
822 bacterial colony (or colonies when applicable) is automatically segmented using a user-defined
823 threshold intensity value. Finally, the image background is changed to plain white for display
824 purposes. When applicable, the script calculated the seeding distance between different species
825 as the Euclidean distance between two positions, defined by the user based on the distinct
826 appearance of the inoculum zones. For each case, the segmentation results were manually
827 validated and corrected using Image J manual tools when necessary.
828
829 Custom MATLAB scripts were used for the coarse-grained kinetic model simulations and
830 the corresponding analyses.
831

Coarse-grained kinetic model

Pseudomonas cell density time change:

$$\frac{\partial P}{\partial t} = \frac{\int_{\Omega} \alpha_P G_P P dx}{\int_{\Omega} dx}$$

where P is *Pseudomonas* cell density (cell density unit: cu), α_P is the growth rate constant of *Pseudomonas* (1/h), Ω indicates the entire colony domain, $\int_{\Omega}$ indicates an integral over the entire colony domain. G_P is the *Pseudomonas* growth function as defined below,

$$G_P = \frac{N}{N + K_N} \frac{C_m}{C_m + P + E} \left(1 - \frac{P + E}{K_C}\right)$$

where N is the local nutrient (casamino acids) concentration (g/l), K_N is the local nutrient concentration for half-maximum growth rate (g/l), C_m is the local cell density for the half-maximum suppression of the growth rate (cu), P is the local *Pseudomonas* cell density (cu), E is the local *Klebsiella* cell density (cu), and K_C is the local carrying capacity (cu).

Pseudomonas branch extension:

$$\frac{dL_i}{dt} = \frac{\gamma}{W} \int_{\Omega_i} \alpha_P G_P P \frac{A_C^h}{A_C^h + A^h} dx$$

where L_i is the length of branch i (mm), γ *Pseudomonas* spatial expansion efficiency (mm/(h.cu)), W is the branch width previously measured from experimental data (mm)[58], A is the local cefotaxime antibiotic concentration (mol/l), A_C is cefotaxime concentration for half-maximum suppression of *Pseudomonas* effective spatial expansion ability (mol/l), h is the steepness of the suppression of *Pseudomonas* effective spatial expansion ability by cefotaxime, Ω_i indicates the domain of branch i, and $\int_{\Omega_i}$ indicates an integral over branch i domain.

Klebsiella cell density time change:

$$\frac{\partial E}{\partial t} = \alpha_P (G_E - L_E) E + D_E \nabla^2 E$$

where D_E is the diffusive dispersal rate of *Klebsiella* (mm^2/h), and G_E and L_E are *Klebsiella* growth and lysis functions, respectively, as defined below.

$$G_E = \mu_E G_P$$

where μ_E is the growth rate constant of *Klebsiella* in proportion to that of *Pseudomonas*.

$$L_E = \phi_E G_E \frac{A^{h_2}}{A_E^{h_2} + A^{h_2}}$$

where ϕ_E is the proportionality constant between the growth and lysis rates of *Klebsiella*, A_E is cefotaxime concentration for half-maximum *Klebsiella* lysis rate (mol/l), and h_2 is the steepness of the onset of *Klebsiella* lysis by cefotaxime.

Nutrient concentration time change: $$\frac{\partial N}{\partial t} = -\beta_N G_P P - \beta_{EN} G_E E + D_N \nabla^2 N$$

where β_N and β_{EN} are the rate constants for nutrient consumption by *Pseudomonas* and *Klebsiella*, respectively, cell density growth (g/(l.h.cu) for both). Note that β_{EN} must be constrained tightly as *Pseudomonas* would otherwise avoid *Klebsiella*-colonized territory due to nutrient depletion. D_N is the diffusivity of nutrients (mm^2/h).

Antibiotic concentration time change: $$\frac{\partial A}{\partial t} = -\kappa_B B A + D_A \nabla^2 A$$

where B is the local concentration of extracellular Bla (mol/l), κ_B is the rate constant for cefotaxime antibiotic degradation by Bla (l/(mol.h)), and D_A is the diffusivity of antibiotics (mm^2/h).

Extracellular Bla concentration time change $$\frac{\partial B}{\partial t} = \alpha_P L_E B_{in} E - d_B B + D_B \nabla^2 B$$

where B_{in} is the intracellular concentration of Bla (mol/cell; for *Klebsiella* only), d_B is the spontaneous degradation rate constant for Bla (1/h), and D_B is the diffusivity of Bla (mm^2/h).

We have formulated the above mathematical model building upon our previous models for *Pseudomonas* branching pattern formation[58] and Bla-producing bacteria population dynamics under β-lactam treatment[45]:

As we lack a complete mechanistic understanding of how *Pseudomonas* colonies develop branches, our model defines the colony morphology formation based on a set of explicit rules, as described by Luo, *et al*.[58]: (1) A colony initiates from a circular inoculum. (2) Branches emerge with a defined branch width *W* and branch density *D* (number of branch tips per unit area), both measured from experimental data. (3) Each branch i extends at an extension rate dL_i/dt, which is proportional to cell growth within the branch. (4) Each branch extends following the local nutrient gradient (towards where the nutrient concentration increases most steeply) and bifurcates when the local cell density reaches the threshold *D*.

At each timestep, we compute cell growth, nutrient consumption, antibiotics degradation, etc., and determine the extension rate from cell growth using the equations described above. For simplicity, we assume that the cell density redistributes and becomes uniform within the colony at each timestep.

Based on this framework, we incorporated antibiotic inhibition into the branch extension to account for the effect of antibiotics on colony expansion. Also, from our previous model for Bla-producing bacteria population dynamics under β-lactam treatment[45], we incorporated *Klebsiella* growth and lysis due to antibiotics, Bla production by lysing *Klebsiella*, and antibiotic degradation by Bla.

We used the parameter values from the two original papers[45,58], with some minor modifications, when possible. The diffusivities of the antibiotic and Bla were chosen based on their molecular weights relative to nutrients (i.e., casamino acids), as suggested by Einstein's relation. The parameter values for the cefotaxime concentration for the half-maximum suppression of *Pseudomonas*' effective spatial expansion ability (A_C) and the sharpness of this suppression (h) were used from the Hill-fits to our experimental data above (see Supplementary Fig. 9a caption).

We assumed no spontaneous degradation of the antibiotic or nutrient recycling after lysis. Finally, we added another parameter to account for our experimental observation above that *Pseudomonas* spatial expansion is effectively biased towards *Klebsiella* (Fig. 2b and Supplementary Fig. 14). This parameter essentially determines the relative dominance of *Pseudomonas*' range expansion on nutrient gradients versus antibiotic gradients depending on their global profiles: *Pseudomonas* would move towards decreasing antibiotic concentration (i.e.,

925 the *Klebsiella* neighborhood), except when $d = 0$, if the spatial global average of antibiotic
926 concentration is greater than A_C and if the global minimum of nutrient concentration is greater
927 than a factor (A_g = 0.7 as the default value) of the nutrient concentration for half maximum specific
928 growth rate (K_N). For $d = 0$, this factor was applied as A_g = 10^{16} to represent an infinitely large
929 value.
930
931 The partial differential equations were numerically solved using a custom MATLAB
932 implementation of the alternating direction implicit method by applying no-flux boundary
933 conditions. The numerical simulations were run in a 1001-by-1001-pixel spatial domain, where
934 each pixel dimension was equivalent to a ~ 0.106 mm spatial length based on the model
935 parameters used. Each population was started in a circular zone equivalent of 5 mm radius. The
936 simulation timestep used was equivalent to 0.02 h, again, based on the model parameters used.
937
938 See Supplementary Table 2 for the values of the model parameters as well as the initial
939 conditions used.
940

941 **Acknowledgments**

942 We thank Lawrence A. David, Joanna B. Goldberg, David K. Karig, Jeffrey Letourneau,
943 Jia Lu, Alice S. Prince, and David S. Weiss for helpful feedback. We thank Yasa Baig, Minsu Kim,
944 Philip N. Rather, and Stuart A. West for their critical reading of an earlier version of the manuscript.
945 This work was partially supported by grants from National Institutes of Health (LY:
946 R01GM098642), Office of Naval Research (LY: N00014-20-1-2121), Defense Advanced
947 Research Projects Agency (LY: 2501-203-2015861), National Science Foundation (LY & CTL:
948 MCB-1937259), and by the Engineering Research Centers Program of the National Science
949 Foundation under NSF Cooperative Agreement No. EEC-2133504. The funders had no role in
950 study design, data collection and analysis, decision to publish, or preparation of the manuscript.
951
952
953 **Author contributions**

954 E. Ş.: Conceived the study, designed, and conducted the research. Wrote the manuscript.
955 C. A. V.: Assisted with experiments in Fig. 1 and Supplementary Fig. 10. K. S.: Assisted with
956 experiments in Supplementary Fig. 13. Z. Z. Assisted with experiments in Supplementary Fig. 8a
957 and Supplementary Fig. 21a. Wrote the cylindrically symmetric antibiotic gradient solution in the
958 Supplementary Information. N. L.: Made observations that inspired this study. D. L.: Constructed
959 the fluorescent protein-labeled variant of *Klebsiella* (*Klebsiella*-mCherry). Assisted in the
960 experiments that led to Supplementary Fig. 10. H. R. M.: Assisted in the isolation of the hospital
961 sink bacteria. D. J. A.: Obtained and provided the p-trap water samples which led to the isolation

of the hospital sink bacteria. C. T. L.: Assisted with data interpretation, writing the manuscript, and articulating the broader ecological context. L. Y.: Conceived the study and assisted with research design and data interpretation. Wrote the manuscript.

All authors contributed to the reviewing and editing of manuscript drafts and approved the final version.

Conflicts of interest

None are declared.

Data availability

Sequencing data supporting Fig. 4, Supplementary Fig. 26, and Supplementary Table 1 are available at 10.5281/zenodo.15882541. Data supporting Supplementary Fig. 5,9,10,13,14,19,24,25 are also available at 10.5281/zenodo.15882541. All other data are provided in the main text, supplementary material, or at https://github.com/youlab/keystone.

Code availability

Codes are available at https://github.com/youlab/keystone.

References

1 Paine, R. T. A Note on Trophic Complexity and Community Stability. *Am Nat* **103**, 91-93 (1969). https://doi.org/10.1086/282586

2 Power, M. E. *et al.* Challenges in the Quest for Keystones. *BioScience* **46**, 609-620 (1996). https://doi.org/10.2307/1312990

3 Jones, C. G., Lawton, J. H. & Shachak, M. Organisms as Ecosystem Engineers. *Oikos* **69**, 373-386 (1994). https://doi.org/10.2307/3545850

4 Hastings, A. *et al.* Ecosystem engineering in space and time. *Ecol Lett* **10**, 153-164 (2007). https://doi.org/https://doi.org/10.1111/j.1461-0248.2006.00997.x

5 Duchardt, C. J., Porensky, L. M. & Pearse, I. S. Direct and indirect effects of a keystone engineer on a shrubland-prairie food web. *Ecology* **102**, e03195 (2021). https://doi.org/https://doi.org/10.1002/ecy.3195

6 Yeakel, J. D. *et al.* Diverse interactions and ecosystem engineering can stabilize community assembly. *Nat Commun* **11**, 3307 (2020). https://doi.org/10.1038/s41467-020-17164-x

7 Carlström, C. I. *et al.* Synthetic microbiota reveal priority effects and keystone strains in the Arabidopsis phyllosphere. *Nature Ecology & Evolution* **3**, 1445-1454 (2019). https://doi.org/10.1038/s41559-019-0994-z

8 Banerjee, S., Schlaeppi, K. & van der Heijden, M. G. A. Keystone taxa as drivers of microbiome structure and functioning. *Nature Reviews Microbiology* **16**, 567-576 (2018). https://doi.org/10.1038/s41579-018-0024-1

9 Losapio, G., Genes, L., Knight, C. J., McFadden, T. N. & Pavan, L. Monitoring and modelling the effects of ecosystem engineers on ecosystem functioning. *Functional Ecology* **n/a** https://doi.org/https://doi.org/10.1111/1365-2435.14315

10 Harvey, E., Gounand, I., Ward, C. L. & Altermatt, F. Bridging ecology and conservation: from ecological networks to ecosystem function. *Journal of Applied Ecology* **54**, 371-379 (2017). https://doi.org/https://doi.org/10.1111/1365-2664.12769

11 Boogert, N. J., Paterson, D. M. & Laland, K. N. The Implications of Niche Construction and Ecosystem Engineering for Conservation Biology. *BioScience* **56**, 570-578 (2006). https://doi.org/10.1641/0006-3568(2006)56[570:Tionca]2.0.Co;2

12 Sadiq, F. A. *et al.* Dynamic social interactions and keystone species shape the diversity and stability of mixed-species biofilms – an example from dairy isolates. *ISME Communications* **3** (2023). https://doi.org/10.1038/s43705-023-00328-3

13 Sun, X. *et al.* Metabolic interactions affect the biomass of synthetic bacterial biofilm communities. *mSystems* **8**, e01045-01023 (2023). https://doi.org/doi:10.1128/msystems.01045-23

14 Ze, X., Duncan, S. H., Louis, P. & Flint, H. J. Ruminococcus bromii is a keystone species for the degradation of resistant starch in the human colon. *ISME J* **6**, 1535-1543 (2012). https://doi.org/10.1038/ismej.2012.4

15 Kropp, C. *et al.* The Keystone commensal bacterium Christensenella minuta DSM 22607 displays anti-inflammatory properties both in vitro and in vivo. *Sci Rep* **11**, 11494 (2021). https://doi.org/10.1038/s41598-021-90885-1

16 Hajishengallis, G. *et al.* Low-Abundance Biofilm Species Orchestrates Inflammatory Periodontal Disease through the Commensal Microbiota and Complement. *Cell Host & Microbe* **10**, 497-506 (2011). https://doi.org/10.1016/j.chom.2011.10.006

17 Flynn, J. M., Niccum, D., Dunitz, J. M. & Hunter, R. C. Evidence and Role for Bacterial Mucin Degradation in Cystic Fibrosis Airway Disease. *PLoS Pathog* **12**, e1005846 (2016). https://doi.org/10.1371/journal.ppat.1005846

1029 18 Großkopf, T. & Soyer, O. S. Synthetic microbial communities. *Curr Opin Microbiol* **18**, 72-
1030 77 (2014). https://doi.org/https://doi.org/10.1016/j.mib.2014.02.002
1031 19 Friedman, J., Higgins, L. M. & Gore, J. Community structure follows simple assembly rules
1032 in microbial microcosms. *Nature Ecology & Evolution* **1**, 0109 (2017).
1033 https://doi.org/10.1038/s41559-017-0109
1034 20 Chang, C.-Y., Bajić, D., Vila, J. C. C., Estrela, S. & Sanchez, A. Emergent coexistence in
1035 multispecies microbial communities. *Science* **381**, 343-348 (2023).
1036 https://doi.org/doi:10.1126/science.adg0727
1037 21 Clerc, E. E. *et al.* Chemotaxis, growth, and inter-species interactions shape early bacterial
1038 community assembly. *ISME J* **19** (2025). https://doi.org/10.1093/ismejo/wraf101
1039 22 Humphries, J. *et al.* Species-Independent Attraction to Biofilms through Electrical
1040 Signaling. *Cell* **168**, 200-209.e212 (2017). https://doi.org/10.1016/j.cell.2016.12.014
1041 23 Amor, D. R., Ratzke, C. & Gore, J. Transient invaders can induce shifts between
1042 alternative stable states of microbial communities. *Science Advances* **6**, eaay8676 (2020).
1043 https://doi.org/doi:10.1126/sciadv.aay8676
1044 24 Weiss, A. S. *et al.* Nutritional and host environments determine community ecology and
1045 keystone species in a synthetic gut bacterial community. *Nat Commun* **14**, 4780 (2023).
1046 https://doi.org/10.1038/s41467-023-40372-0
1047 25 Niu, B., Paulson, J. N., Zheng, X. & Kolter, R. Simplified and representative bacterial
1048 community of maize roots. *Proceedings of the National Academy of Sciences* **114**, E2450-
1049 E2459 (2017). https://doi.org/doi:10.1073/pnas.1616148114
1050 26 Lee, K. W. K. *et al.* Biofilm development and enhanced stress resistance of a model,
1051 mixed-species community biofilm. *ISME J* **8**, 894-907 (2014).
1052 https://doi.org/10.1038/ismej.2013.194
1053 27 Wicaksono, W. A. *et al.* Enhanced survival of multi-species biofilms under stress is
1054 promoted by low-abundant but antimicrobial-resistant keystone species. *Journal of*
1055 *Hazardous Materials* **422**, 126836 (2022).
1056 https://doi.org/https://doi.org/10.1016/j.jhazmat.2021.126836
1057 28 Centanni, M. *et al.* Bifidobacterium pseudolongum in the Ceca of Rats Fed Hi-Maize
1058 Starch Has Characteristics of a Keystone Species in Bifidobacterial Blooms. *Appl Environ*
1059 *Microbiol* **84**, e00547-00518 (2018). https://doi.org/doi:10.1128/AEM.00547-18
1060 29 Cartmell, A. *et al.* A surface endogalactanase in Bacteroides thetaiotaomicron confers
1061 keystone status for arabinogalactan degradation. *Nat Microbiol* **3**, 1314-1326 (2018).
1062 https://doi.org/10.1038/s41564-018-0258-8

1063 30 Chng, K. R. *et al.* Metagenome-wide association analysis identifies microbial determinants
1064 of post-antibiotic ecological recovery in the gut. *Nature Ecology & Evolution* **4**, 1256-1267
1065 (2020). https://doi.org/10.1038/s41559-020-1236-0
1066 31 Feng, J. *et al.* Polysaccharide utilization loci in Bacteroides determine
1067 population fitness and community-level interactions. *Cell Host & Microbe* **30**, 200-
1068 215.e212 (2022). https://doi.org/10.1016/j.chom.2021.12.006
1069 32 Hajishengallis, G., Darveau, R. P. & Curtis, M. A. The keystone-pathogen hypothesis.
1070 *Nature Reviews Microbiology* **10**, 717-725 (2012). https://doi.org/10.1038/nrmicro2873
1071 33 Hajishengallis, G. & Lamont, R. J. Dancing with the Stars: How Choreographed Bacterial
1072 Interactions Dictate Nososymbiocity and Give Rise to Keystone Pathogens, Accessory
1073 Pathogens, and Pathobionts. *Trends Microbiol* **24**, 477-489 (2016).
1074 https://doi.org/10.1016/j.tim.2016.02.010
1075 34 Fenchel, T. Microbial Behavior in a Heterogeneous World. *Science* **296**, 1068-1071
1076 (2002). https://doi.org/doi:10.1126/science.1070118
1077 35 Costerton, J. W., Geesey, G. G. & Cheng, K. J. How bacteria stick. *Sci Am* **238**, 86-95
1078 (1978). https://doi.org/10.1038/scientificamerican0178-86
1079 36 Or, D., Smets, B. F., Wraith, J. M., Dechesne, A. & Friedman, S. P. Physical constraints
1080 affecting bacterial habitats and activity in unsaturated porous media – a review. *Advances*
1081 *in Water Resources* **30**, 1505-1527 (2007).
1082 https://doi.org/https://doi.org/10.1016/j.advwatres.2006.05.025
1083 37 Le, S. *et al.* Bacteriophage protein Dap1 regulates evasion of antiphage immunity and
1084 Pseudomonas aeruginosa virulence impacting phage therapy in mice. *Nat Microbiol*
1085 (2024). https://doi.org/10.1038/s41564-024-01719-5
1086 38 Mitchell, J. G. & Kogure, K. Bacterial motility: links to the environment and a driving force
1087 for microbial physics. *FEMS Microbiology Ecology* **55**, 3-16 (2006).
1088 https://doi.org/10.1111/j.1574-6941.2005.00003.x
1089 39 Tsao, Y.-F. *et al.* Phage Morons Play an Important Role in Pseudomonas aeruginosa
1090 Phenotypes. *J Bacteriol* **200**, 10.1128/jb.00189-00118 (2018).
1091 https://doi.org/doi:10.1128/jb.00189-18
1092 40 Shah, M. *et al.* A phage-encoded anti-activator inhibits quorum sensing in Pseudomonas
1093 aeruginosa. *Mol Cell* **81**, 571-583.e576 (2021).
1094 https://doi.org/https://doi.org/10.1016/j.molcel.2020.12.011

1095 41 Finkelshtein, A., Roth, D., Jacob, E. B. & Ingham, C. J. Bacterial Swarms Recruit Cargo
1096 Bacteria To Pave the Way in Toxic Environments. *MBio* **6**, 10.1128/mbio.00074-00015
1097 (2015). https://doi.org/doi:10.1128/mbio.00074-15
1098 42 Caiazza, N. C., Shanks, R. M. Q. & O'Toole, G. A. Rhamnolipids Modulate Swarming
1099 Motility Patterns of Pseudomonas aeruginosa. *J Bacteriol* **187**, 7351-7361 (2005).
1100 https://doi.org/doi:10.1128/jb.187.21.7351-7361.2005
1101 43 Luo, N. *et al.* The collapse of cooperation during range expansion of Pseudomonas
1102 aeruginosa. *Nat Microbiol* (2024). https://doi.org/10.1038/s41564-024-01627-8
1103 44 Pradhan, D. *et al.* Toroidal displacement of Klebsiella pneumoniae by
1104 Pseudomonas aeruginosa is a unique mechanism to avoid competition for iron.
1105 *MBio* **0**, e01149-01125 https://doi.org/doi:10.1128/mbio.01149-25
1106 45 Meredith, H. R. *et al.* Applying ecological resistance and resilience to dissect bacterial
1107 antibiotic responses. *Science Advances* **4**, eaau1873 (2018).
1108 https://doi.org/doi:10.1126/sciadv.aau1873
1109 46 Magill, S. S. *et al.* Multistate Point-Prevalence Survey of Health Care–Associated
1110 Infections. *New England Journal of Medicine* **370**, 1198-1208 (2014).
1111 https://doi.org/10.1056/NEJMoa1306801
1112 47 Rennie, R. P., Jones, R. N. & Mutnick, A. H. Occurrence and antimicrobial susceptibility
1113 patterns of pathogens isolated from skin and soft tissue infections: report from the
1114 SENTRY Antimicrobial Surveillance Program (United States and Canada, 2000).
1115 *Diagnostic Microbiology and Infectious Disease* **45**, 287-293 (2003).
1116 https://doi.org/https://doi.org/10.1016/S0732-8893(02)00543-6
1117 48 Marchaim, D. *et al.* “Swimming in resistance”: Co-colonization with carbapenem-resistant
1118 Enterobacteriaceae and Acinetobacter baumannii or Pseudomonas aeruginosa. *American*
1119 *Journal of Infection Control* **40**, 830-835 (2012).
1120 https://doi.org/https://doi.org/10.1016/j.ajic.2011.10.013
1121 49 Palavecino, E., Ramirez, K., Greene, S. R. & Kilic, A. Co-existence of VIM-2-producing
1122 Pseudomonas aeruginosa and KPC-2 and OXA-232-co-producing Klebsiella pneumoniae
1123 in the United States. *Ann Lab Med* **40**, 267-269 (2020).
1124 https://doi.org/10.3343/alm.2020.40.3.267
1125 50 Frank, D. N., Wilson, S. S., St. Amand, A. L. & Pace, N. R. Culture-Independent
1126 Microbiological Analysis of Foley Urinary Catheter Biofilms. *PLoS ONE* **4**, e7811 (2009).
1127 https://doi.org/10.1371/journal.pone.0007811

51 Noorian, P. *et al.* A model, mixed-species urinary catheter biofilm derived from spinal cord injury patients. *BioRxiv*, 2024.2011.2004.621968 (2024). https://doi.org/10.1101/2024.11.04.621968

52 Rashid, M. H. & Kornberg, A. Inorganic polyphosphate is needed for swimming, swarming, and twitching motilities of Pseudomonas aeruginosa. *Proceedings of the National Academy of Sciences* **97**, 4885-4890 (2000). https://doi.org/doi:10.1073/pnas.060030097

53 Arslan, E., Coşkun, M. K., Çobanoğlu, Ş., Aslan, M. H. & Yazıcı, A. Effects of four antibiotics on Pseudomonas aeruginosa motility, biofilm formation, and biofilm-specific antibiotic resistance genes expression. *Diagnostic Microbiology and Infectious Disease* **106**, 115931 (2023). https://doi.org/https://doi.org/10.1016/j.diagmicrobio.2023.115931

54 Kumar, L., Brenner, N., Brice, J., Klein-Seetharaman, J. & Sarkar, S. K. Cephalosporins Interfere With Quorum Sensing and Improve the Ability of Caenorhabditis elegans to Survive Pseudomonas aeruginosa Infection. *Front Microbiol* **12** (2021). https://doi.org/10.3389/fmicb.2021.598498

55 Liu, Y., Lehnert, T. & Gijs, M. A. M. Effect of inoculum size and antibiotics on bacterial traveling bands in a thin microchannel defined by optical adhesive. *Microsystems & Nanoengineering* **7**, 86 (2021). https://doi.org/10.1038/s41378-021-00309-3

56 Oliveira, N. M. *et al.* Suicidal chemotaxis in bacteria. *Nat Commun* **13**, 7608 (2022). https://doi.org/10.1038/s41467-022-35311-4

57 Berg, H. C. *Random Walks in Biology*
New and Expanded Edition. REV - Revised edn, (Princeton University Press, 1993).

58 Luo, N., Wang, S., Lu, J., Ouyang, X. & You, L. Collective colony growth is optimized by branching pattern formation in Pseudomonas aeruginosa. *Mol Syst Biol* **17**, e10089 (2021). https://doi.org/https://doi.org/10.15252/msb.202010089

59 Starlander, G. & Melhus, Å. Minor outbreak of extended-spectrum β-lactamase-producing Klebsiella pneumoniae in an intensive care unit due to a contaminated sink. *Journal of Hospital Infection* **82**, 122-124 (2012). https://doi.org/https://doi.org/10.1016/j.jhin.2012.07.004

60 Hota, S. *et al.* Outbreak of Multidrug-Resistant Pseudomonas aeruginosa Colonization and Infection Secondary to Imperfect Intensive Care Unit Room Design. *Infection Control & Hospital Epidemiology* **30**, 25-33 (2009). https://doi.org/10.1086/592700

61 Kotay, S., Chai, W., Guilford, W., Barry, K. & Mathers, A. J. Spread from the Sink to the Patient: In Situ Study Using Green Fluorescent Protein (GFP)-Expressing Escherichia coli To Model Bacterial Dispersion from Hand-Washing Sink-Trap Reservoirs.

Appl Environ Microbiol **83**, e03327-03316 (2017). https://doi.org/doi:10.1128/AEM.03327-16

62 Tanouchi, Y., Pai, A., Buchler, N. E. & You, L. Programming stress-induced altruistic death in engineered bacteria. *Mol Syst Biol* **8**, 626 (2012). https://doi.org/https://doi.org/10.1038/msb.2012.57

63 Şimşek, E. *et al.* A 'rich-get-richer' mechanism drives patchy dynamics and resistance evolution in antibiotic-treated bacteria. *Mol Syst Biol* **20**, 880-897 (2024). https://doi.org/https://doi.org/10.1038/s44320-024-00046-5

64 Bertness, M. D. & Callaway, R. Positive interactions in communities. *Trends Ecol Evol (Amst)* **9**, 191-193 (1994). https://doi.org/https://doi.org/10.1016/0169-5347(94)90088-4

65 Bronstein, J. L. Conditional outcomes in mutualistic interactions. *Trends Ecol Evol (Amst)* **9**, 214-217 (1994). https://doi.org/https://doi.org/10.1016/0169-5347(94)90246-1

66 Hoek, T. A. *et al.* Resource Availability Modulates the Cooperative and Competitive Nature of a Microbial Cross-Feeding Mutualism. *PLoS Biol* **14**, e1002540 (2016). https://doi.org/10.1371/journal.pbio.1002540

67 Fetzer, I. *et al.* The extent of functional redundancy changes as species' roles shift in different environments. *Proceedings of the National Academy of Sciences* **112**, 14888-14893 (2015). https://doi.org/doi:10.1073/pnas.1505587112

68 Thiery, S. & Kaimer, C. The Predation Strategy of Myxococcus xanthus. *Front Microbiol* **11** (2020). https://doi.org/10.3389/fmicb.2020.00002

69 Elyasi Far, B., Ahmadi, Y., Yari Khosroshahi, A. & Dilmaghani, A. Microbial Alpha-Amylase Production: Progress, Challenges and Perspectives. *Adv Pharm Bull* **10**, 350-358 (2020). https://doi.org/10.34172/apb.2020.043

70 Jin, F., Conrad, J. C., Gibiansky, M. L. & Wong, G. C. L. Bacteria use type-IV pili to slingshot on surfaces. *Proceedings of the National Academy of Sciences* **108**, 12617-12622 (2011). https://doi.org/doi:10.1073/pnas.1105073108

71 Mattick, J. S. Type IV Pili and Twitching Motility. *Annu Rev Microbiol* **56**, 289-314 (2002). https://doi.org/https://doi.org/10.1146/annurev.micro.56.012302.160938

72 Fortune, G. T., Oliveira, N. M. & Goldstein, R. E. Biofilm Growth under Elastic Confinement. *Phys Rev Lett* **128**, 178102 (2022). https://doi.org/10.1103/PhysRevLett.128.178102

73 Seminara, A. *et al.* Osmotic spreading of Bacillus subtilis biofilms driven by an extracellular matrix. *Proceedings of the National Academy of Sciences* **109**, 1116-1121 (2012). https://doi.org/doi:10.1073/pnas.1109261108

1196 74 Zhang, Q. *et al.* Morphogenesis and cell ordering in confined bacterial biofilms.
1197 *Proceedings of the National Academy of Sciences* **118**, e2107107118 (2021).
1198 https://doi.org/doi:10.1073/pnas.2107107118
1199 75 Ma, H. R., Xu, H. Z., Kim, K., Anderson, D. J. & You, L. Private benefit of β-lactamase
1200 dictates selection dynamics of combination antibiotic treatment. *Nat Commun* **15**, 8337
1201 (2024). https://doi.org/10.1038/s41467-024-52711-w
1202 76 Cena, J. A. d., Zhang, J., Deng, D., Damé-Teixeira, N. & Do, T. Low-Abundant
1203 Microorganisms: The Human Microbiome's Dark Matter, a Scoping Review. *Frontiers in*
1204 *Cellular and Infection Microbiology* **11** (2021). https://doi.org/10.3389/fcimb.2021.689197
1205 77 Xavier, J. B., Kim, W. & Foster, K. R. A molecular mechanism that stabilizes cooperative
1206 secretions in Pseudomonas aeruginosa. *Mol Microbiol* **79**, 166-179 (2011).
1207 https://doi.org/10.1111/j.1365-2958.2010.07436.x
1208 78 Fournet-Fayard, S., Joly, B. & Forestier, C. Transformation of wild type Klebsiella
1209 pneumoniae with plasmid DNA by electroporation. *J Microbiol Methods* **24**, 49-54 (1995).
1210 https://doi.org/https://doi.org/10.1016/0167-7012(95)00053-4
1211 79 Payne, S. *et al.* Temporal control of self-organized pattern formation without morphogen
1212 gradients in bacteria. *Mol Syst Biol* **9**, 697 (2013). https://doi.org/10.1038/msb.2013.55
1213 80 Barbier, M. & Damron, F. H. Rainbow Vectors for Broad-Range Bacterial Fluorescence
1214 Labeling. *PLoS ONE* **11**, e0146827 (2016). https://doi.org/10.1371/journal.pone.0146827
1215 81 Santos-Moreno, J., Tasiudi, E., Stelling, J. & Schaerli, Y. Multistable and dynamic
1216 CRISPRi-based synthetic circuits. *Nat Commun* **11**, 2746 (2020).
1217 https://doi.org/10.1038/s41467-020-16574-1
1218 82 Warren, B. G. *et al.* Identification of carbapenem-resistant organism (CRO) contamination
1219 of in-room sinks in intensive care units in a new hospital bed tower. *Infection Control &*
1220 *Hospital Epidemiology* **45**, 302-309 (2024). https://doi.org/10.1017/ice.2023.289
1221 83 Bolyen, E. *et al.* Reproducible, interactive, scalable and extensible microbiome data
1222 science using QIIME 2. *Nature Biotechnology* **37**, 852-857 (2019).
1223 https://doi.org/10.1038/s41587-019-0209-9
1224 84 Martin, M. Cutadapt removes adapter sequences from high-throughput sequencing reads.
1225 *2011* **17**, 3 (2011). https://doi.org/10.14806/ej.17.1.200
1226 85 Callahan, B. J. *et al.* DADA2: High-resolution sample inference from Illumina amplicon
1227 data. *Nat Methods* **13**, 581-583 (2016). https://doi.org/10.1038/nmeth.3869
1228 86 Rognes, T., Flouri, T., Nichols, B., Quince, C. & Mahé, F. VSEARCH: a versatile open
1229 source tool for metagenomics. *PeerJ* **4**, e2584 (2016). https://doi.org/10.7717/peerj.2584

1230 87 Wick, R. R., Judd, L. M., Gorrie, C. L. & Holt, K. E. Unicycler: Resolving bacterial genome
1231 assemblies from short and long sequencing reads. *PLoS Comput Biol* **13**, e1005595
1232 (2017). https://doi.org/10.1371/journal.pcbi.1005595
1233 88 Gurevich, A., Saveliev, V., Vyahhi, N. & Tesler, G. QUAST: quality assessment tool for
1234 genome assemblies. *Bioinformatics* **29**, 1072-1075 (2013).
1235 https://doi.org/10.1093/bioinformatics/btt086
1236 89 Schwengers, O. *et al.* Bakta: rapid and standardized annotation of bacterial genomes via
1237 alignment-free sequence identification. *Microbial Genomics* **7** (2021).
1238 https://doi.org/https://doi.org/10.1099/mgen.0.000685
1239